

CloudSat Project

A NASA Earth System Science Pathfinder Mission

Level 2 Cloud Scenario Classification Product Process Description and Interface Control Document

Version: 5.0

Date: July 24, 2007

Questions concerning the document and proposed changes shall be addressed to

Zhien Wang
University of Wyoming 307-766-5356 OR
zwang@uwyo.edu

Kenneth Sassen
University of Alaska
ksassen@gi.alaska.edu



**Cooperative Institute for Research in the Atmosphere
Colorado State University
Fort Collins, CO 80523**

Contents

Contents	3
1. Introduction	4
2. Algorithm Theoretical Basis	5
3. Algorithm Inputs	12
3.1. CloudSat.....	12
3.1.1. CPR-only Geometric Profiles:	12
3.2. Ancillary (Non-CloudSat).....	13
3.2.1. MODIS.....	13
3.2.2. ECMWF.....	13
3.2.3. Coastline Map	13
3.2.4. Topographical Map.....	13
3.3. Input Variable Summary	14
3.4. Control and Calibration.....	19
4. Algorithm Summary	20
4.1. Cloud clustering analysis	20
4.2. The flowchart of cloud scenario classification	22
4.3. Precipitation Identification.....	23
4.4. Role-based Cloud Classification.....	29
5. Data Product Output Format	37
5.1. Product Field Specifications	37
6. Operator Instructions	43
7. References	47
8. Acronym List	49
9. Open Issues	49
10. Major changes since version 4.0	50

1. Introduction

A great strength of microwave radar measurements of clouds and precipitation is the ability to retrieve quantitative content data from the radar reflectivity factor Z . This is made possible by devising algorithms based on empirical relationships between Z and various microphysical parameters, such as ice water content IWC or rainfall rate, or based on multiple sensor approaches by combining Z with other measurements. However, because of the diversity of microphysical conditions found in the atmosphere, algorithms need to be applied only to those conditions for which they are considered valid. In other words, it is first necessary to identify the target and then select an appropriate algorithm. The algorithm selection process depends on such basic factors as cloud phase, and also the hydrometeor density, shape, and size distribution. For example, although cirrus, altostratus, and the upper portions of cumulonimbus clouds are all predominantly ice phase clouds, it is not possible to apply a single algorithm for retrieving IWC in these targets: cirrus generally contain only single ice crystals, altostratus likely contain low-density ice crystal aggregates at the warmer temperatures, and cumulonimbus may combine ice crystals, snowflakes, rimed particles, graupel, and even hailstones.

Different types of clouds are usually governed by different cloud dynamics processes and have different microphysical properties, which result in different cloud radiative forcings (Hartmann et al. 1992; Chen et al. 2000). Climate changes can result in changing frequency of cloud type and changing properties of a cloud type. The combination of them determines the change of the role of clouds in the Earth water and energy cycles. We might face difficulties to accurately predict future climate change until climate models can properly represent the processes and feedback mechanisms of controlling different cloud types and their properties. Therefore, classifying clouds into categories based on type is also an important task for cloud remote sensing and global cloud climatology studies.

As the first step in converting the vertical profiles of Z from CloudSat into meaningful microphysical data quantities, we are developing an algorithm for identifying cloud type and precipitation from the information expected to be available. As described here, we identify eight basic cloud types that are recognized by surface observers internationally. Currently, we are relying on CloudSat radar-only Z measurements for cloud identification, but further refinements will incorporate ancillary data such as are available from Aqua and CALIPSO.

Our initial approach is to use an extended cloud dataset obtained over a 1-year period from the Southern Great Plains Clouds and Radiation Testbed site, which identifies these cloud types using a previously developed multiple remote sensor algorithm (Wang and Sassen 2001). We then examine the MMCR (8.7-mm radar) data for each of the identified cloud types to establish relations between the maximum Z_{\max} measured in a particular vertical profile and the temperature at that level. Permissible bounds in temperature and Z_{\max} for each cloud type are established. The horizontal consistency of

the Z_{\max} and horizontal cloud structure are also considered, as well as the presence of precipitation.

2. Algorithm Theoretical Basis

Algorithms based on different cloud spectral, textural, and physical features have been developed for cloud classification from satellites (Welch et al. 1992; Tovinkere et al. 1993; Bankert 1994; Luo et al. 1995; Rossow and Schiffer 1999). The International Satellite Cloud Climatology Project (ISCCP) approach (Rossow and Schiffer 1999) uses the combination of cloud top pressure and cloud optical depth to classify clouds into either cumulus (Cu), stratocumulus (Sc), stratus (St), altocumulus (Ac), altostratus (As), nimbostratus (Ns), cirrus, cirrostratus, or deep convective clouds. Table 1 shows the basic features of these different cloud types (WMO 1956; Parker 1988; Uddstrom and Gray 1996; Moran et al. 1997). However, with more long-term ground-based active and passive remote sensing cloud studies underway, algorithms to classify cloud type using these measurements are developed. Wang and Sassen (2001) developed an algorithm to classify clouds by combining the measurements of ground-based multiple remote sensors. Duchon and O'Malley (1999) studied the possibility of classifying clouds according to ground-based solar flux measurements. Williams et al. (1995) developed an algorithm to classify precipitating clouds into either stratiform, mixed stratiform, convective, and deep or shallow convective clouds using 915-MHz wind profile data.

In this document, we present a new algorithm for CloudSat to classify clouds into either St, Sc, Cu, Ns, Ac, As, deep convective, or high cloud by combining space-based active (CPR and CALIPSO lidar) and passive remote sensing (MODIS) data. The class of high cloud includes cirrus, cirrocumulus, and cirrostratus, and the class of Cu cloud represents cumulus congestus and fair weather cumulus. These types may be further classified into sub-types for IWC and LWC retrievals.

Table 1 Characteristic cloud features for the major cloud types derived from numerous studies (midlatitude). Our cloud type identification algorithm is based on many of these characteristics. Heights are above ground level.

Cloud Class	Cloud Features	
High Cloud	Base	> 7.0 km
	Rain	no
	Horiz. Dim.	10 ³ km
	Vert. Dim.	moderate
	LWP	= 0.
As	Base	2.0-7.0 km
	Rain	none
	Horiz. Dim.	10 ³ km, homogeneous
	Vert. Dim.	moderate
	LWP	~ 0, dominated by ice
Ac	Base	2.0-7.0 km
	Rain	virga possible
	Horiz. Dim.	10 ³ km, inhomogeneous
	Vert. Dim.	shallow or moderate
	LWP	> 0
St	Base	0-2.0 km
	Rain	none or slight
	Horiz. Dim.	10 ² km, homogeneous
	Vert. Dim.	shallow
	LWP	> 0.
Sc	Base	0.-2.0 km
	Rain	drizzle or snow possible
	Horiz. Dim.	10 ³ km, inhomogeneous
	Vert. Dim.	shallow
	LWP	> 0.
Cu	Base	0-3.0 km
	Rain	drizzle or snow possible
	Horiz. Dim.	1 km, isolated
	Vert. Dim.	shallow or moderate
	LWP	> 0.
Ns	Base	0-4.0 km
	Rain	prolonged rain or snow
	Horiz. Dim.	10 ³ km
	Vert. Dim.	thick
	LWP	> 0.
Deep convective clouds	Base	0-3.0 km
	Rain	intense shower of rain or hail possible
	Horiz. Dim.	10 km
	Vert. Dim.	thick
	LWP	> 0.

a. Measurements used for cloud classification

We classify clouds by using vertical and horizontal cloud properties, the presence or absence of precipitation, cloud temperature, and upward radiance from MODIS measurements. Space-based radar and lidar provide vertical cloud profiles and horizontal extent of clouds, which provide important information for differentiating cloud types. Figure 1 shows an example of CloudSat CPR measurements and cloud mask results. Figure 2 presents collocated CloudSat CPR and CALIPSO lidar measurements. These figures show horizontal and vertical variability for different types of clouds. As indicated in Fig. 2, lidar and radar have different advantages to measure different types of clouds from space. Lidar is more sensitive to detect optically thin upper tropospheric clouds and radar provided a better coverage for optically thick clouds. They compliment with each other well. However, the algorithm discussed in this document will use CloudSat CPR measurement only. Combined radar-lidar cloud classification product will be discussed in a separated document.

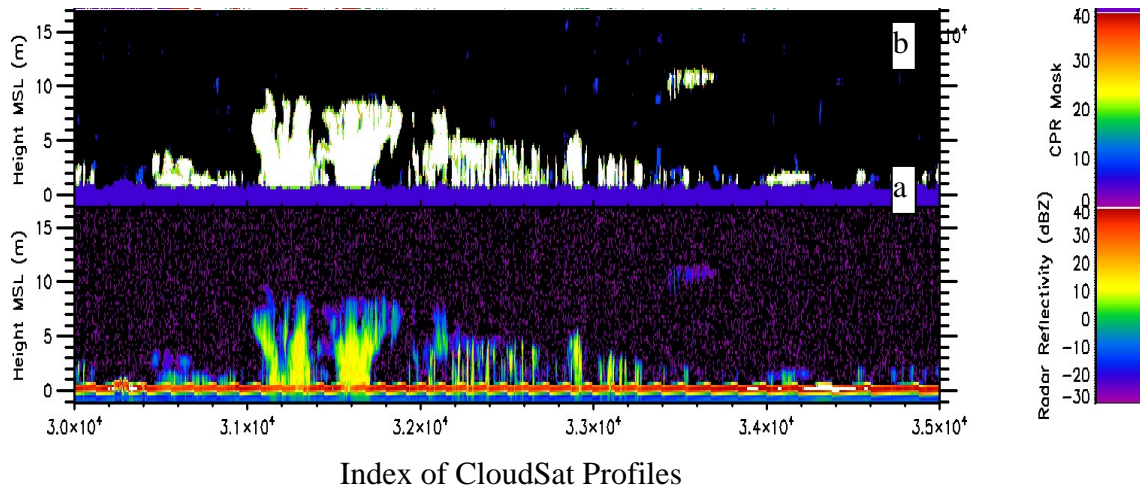


Figure 1: An example of CloudSat measured radar reflectivity factor (a) and cloud mask results (b) from 2B-GEOPROF product.

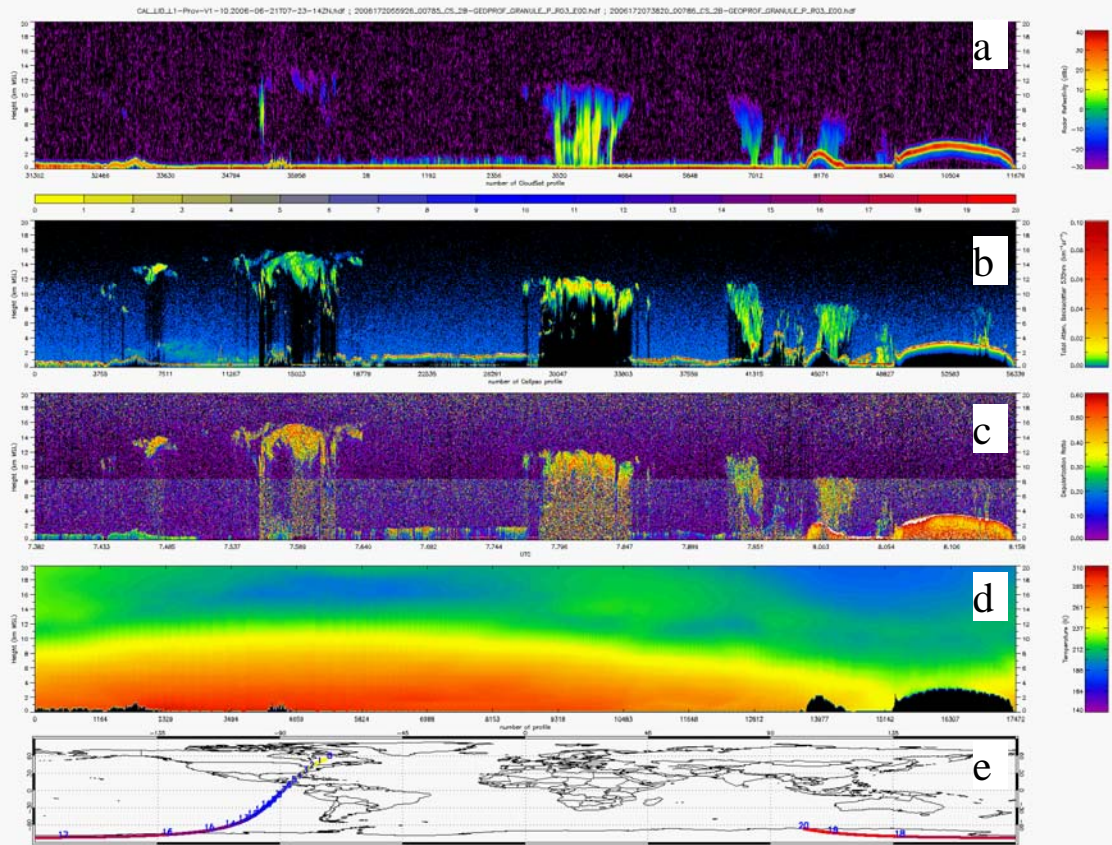


Figure 2: Colocated CloudSat radar (a), CALIPSO attenuated backscattering coefficient (b) and depolarization ratio (c), ECMWF temperature profile (d), and CloudSat track (e).

In addition to active remote sensing data, radiances from MODIS measurements in Aqua could be incorporated into the algorithm. Cloud spectral, and textural features derived from radiance data are important supplementary information to cloud vertical and horizontal extents from active remote sensors. However, column integrated MODIS signals only provide very limited information to characterize multiple-layer clouds.

Cloud temperature (T) derived from ECMWF predictions is an important cloud property. Using our ground-based cloud classification results (Wang and Sassen 2001), we derive the occurrence of different cloud types in maximum Z_e and T (at maximum Z_e height) space (see Fig. 3a and 3b). The features displayed in Fig. 3 are consistent with cloud physics and the microphysical properties of different cloud types. The rules derived from Fig. 3 are showed in Table 2, and are used as an *initial step* to develop Radar-only cloud classification algorithm and more complex rule based classification is developed based on CloudSat data (see section 4).

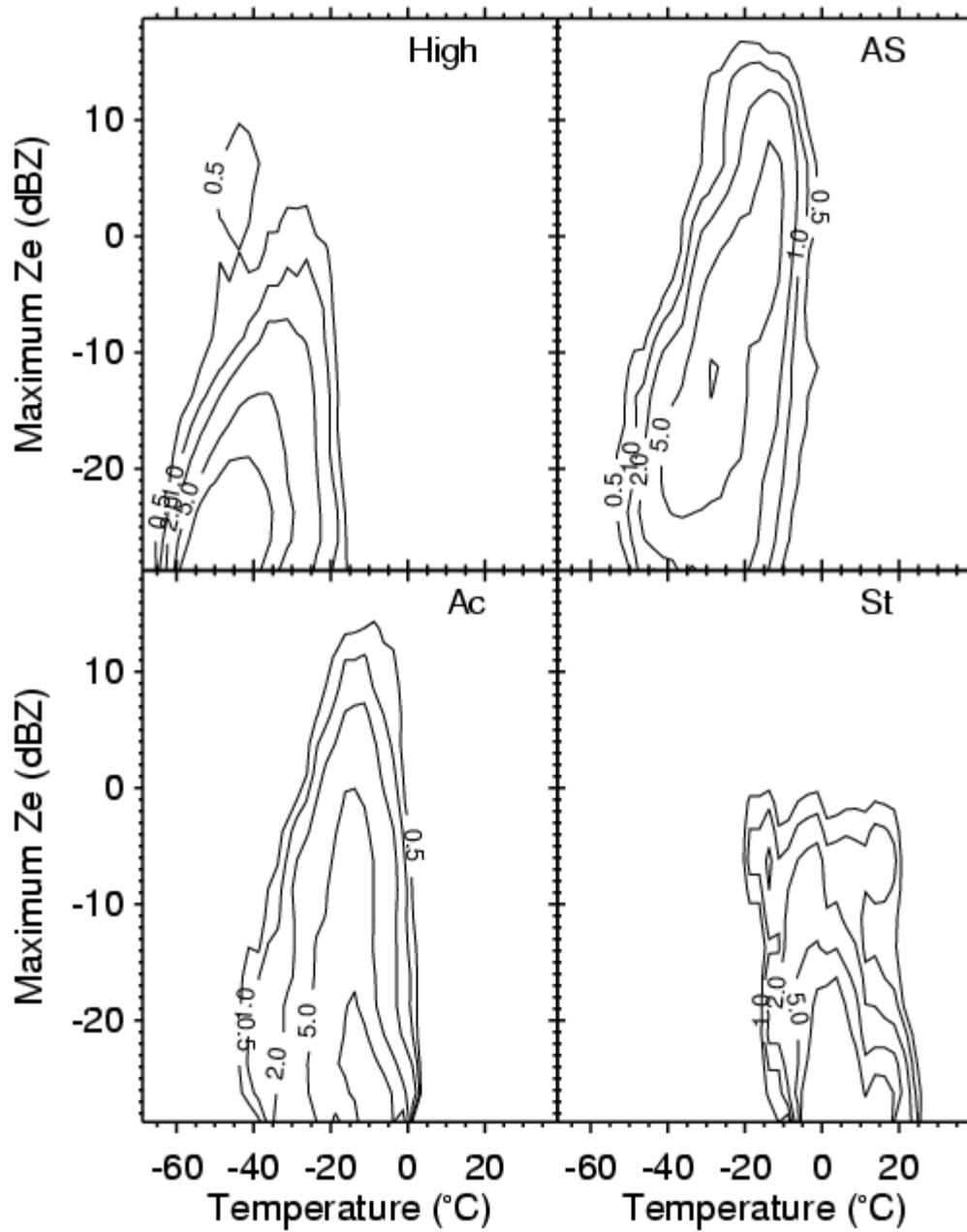


Figure 3a: The occurrence of different type clouds in temperature and maximum Z_e space.

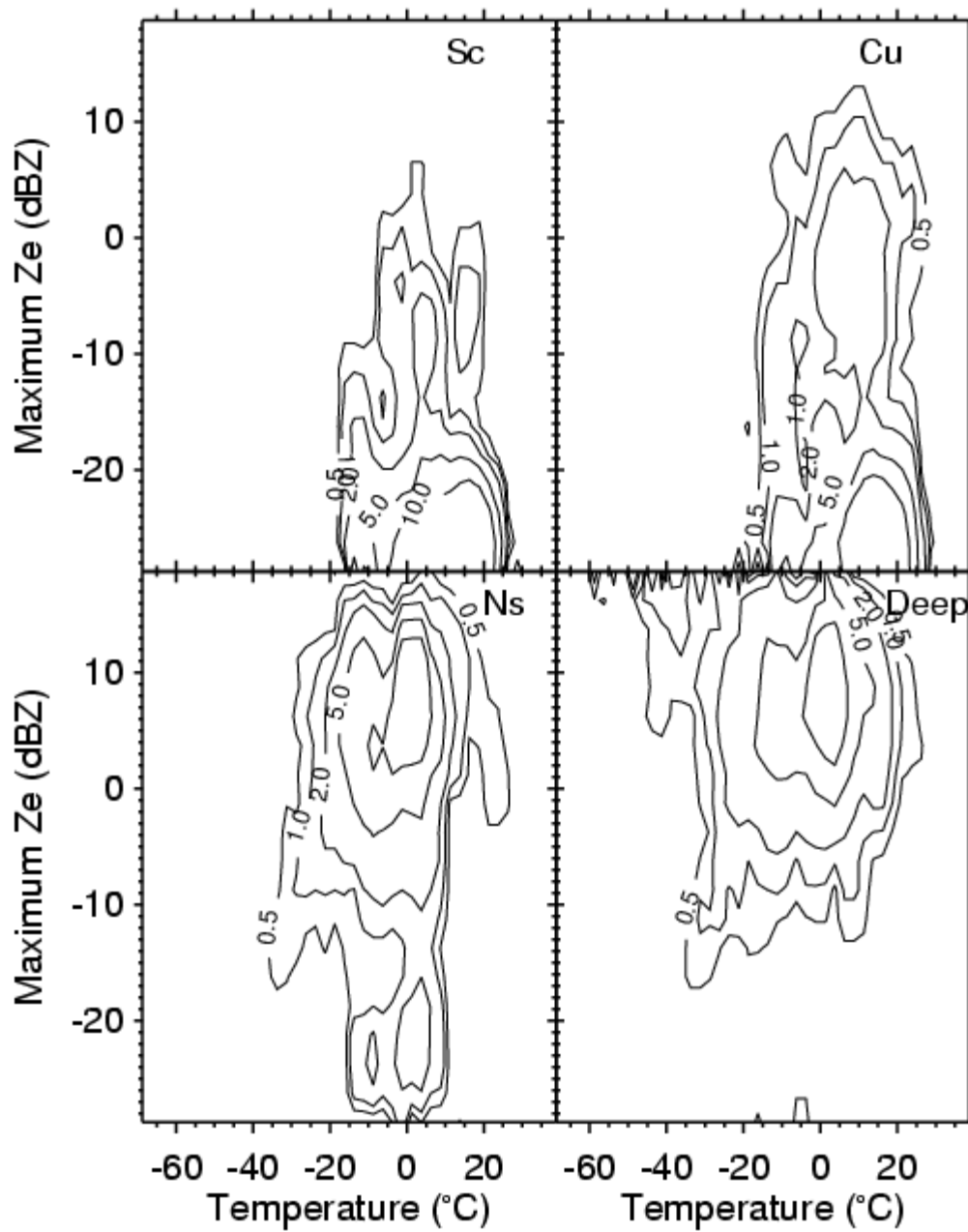


Figure 3b: The occurrence of different type clouds in temperature and maximum Z_e space.

Table 2: Tentative cloud ID rules based approximately on the properties for the 98th percentile of the data shown in Figure 3.

Type	Z _{max}	Precipitation	Length (km)	Highest Z _{max} frequency	Other
Cirrus	<-3 dBZ, T < -22.5°C	No	2→>1000	-25 dBZ @ -40 °C	
Altostratus	<10dBZ, -20° < T < -5 °C; = -30dBZ @ -45 °C	No	50→>1000	-10 dBZ @ -25 °C	
Alto cumulus	<0 dBZ, -20° < T < -5 °C; = -30 dBZ @ -35 °C	Yes/No	2→ >1000	-25 dBZ @ -10 °C	T _{top} > -35 °C
St	<-5 dBZ, -15° < T < 25 °C	Yes/No	50→>1000	-25 dBZ @ 10 °C (Bright band)	Altitude of Z _{max} < 2 km AGL
Sc	<-5 dBZ, -15° < T < 25 °C	Yes/No	2→ >1000	-25 dBZ @ 10 °C (Bright band)	Altitude of Z _{max} < 2 km AGL; spatially inhomogeneous
Cumulus	< 0dBZ, -5° < T < 25 °C	Yes/No	2-25	-25 dBZ @ 15 °C	ΔZ > 2 km
Deep (cb)	>-5dBZ, -20° < T < 25 °C	Yes	10-50	10 dBZ @ 5 °C	ΔZ > 6 km
Ns	-10 < Z < 15 dBZ, -25 ° < T < 10 ° C	Yes	>100	+5 dBZ @ 0 °C	ΔZ > 4 km

b. Methodology

Role-based classification methods, which assigns different threshold values to characteristic parameters, are simple and easy to use methods, but the results are sensitive to the selection of the thresholds. Instead of using Boolean logic, the proper use of fuzzy logic can improve the results of cloud classification (Penoloza and Welch 1996). The approach of using neural networks to classify cloud type in satellite imagery has shown recent success (Welch et al. 1992; Bankert 1994). The network is trained on selected spectral, textural, and physical features associated with expertly labeled samples. The trained network is subsequently applied to unknown cloud samples. However, these new classification techniques can not guarantee better performance, which depends on how properly designed the classifier is and the selection of features (Tovinkere et al. 1993).

Combined rule-based and fuzzy logic classification approach is under development (Wang and Sassen 2004), but radar-only cloud classification discussed here mainly use rule-based classification. We use the following strategy to classify clouds. First, radar cloud mask results are used to find a cloud cluster according to their persistence in the horizontal and vertical directions. A minimum horizontal extent for a cluster is required, therefore, a cloud cluster permits spatially broken cloud fields.

Once a cloud cluster is found, cloud height, temperature, and maximum Z_e , as well as the occurrence of precipitation, are determined. The clouds with precipitation will be classified as either Ns, St, Sc, Ac, or deep convective cloud according to its vertical and horizontal extent, maximum Z_e , and horizontal extent of the precipitation (see Table 1 and 2). A non-precipitating cloud cluster is passed to a high, middle, or low classifier according to its mean cloud height and temperature.

3. Algorithm Inputs

3.1. CloudSat

3.1.1. CPR-only Geometric Profiles:

CPR-only geometric profiles, which provide horizontal and vertical cloud structure, are main inputs for cloud scenario classification. Inputs from CPR-only geometric profiles are (see *Level 2 CPR-only geometric profiles product process description and interface control document*)

Z_e profile

Cloud Mask

Geolocation

Altitude of each radar bin

Surface bin number

3.2. Ancillary (Non-CloudSat)

3.2.1. MODIS

At this point, we plan to use MODIS radiance data of channel 1, 2, 26, 29, 31, and 32 (Ackerman et al. 1998) as supplementary information to CloudSat radar measurements for cloud scenario classification. Currently, we plan to search mainly for cloud variability from the MODIS radiance data orthogonal to the radar ground track.

Table 3: The MODIS bands used in the MODIS cloud mask algorithm

Band	Wavelength (μm)	
1 (250 m)	0.659	Clouds, shadow
2 (250 m)	0.865	low clouds
26	1.375	thin cirrus
29	8.550	cloud
31	11.030	cloud
32	12.020	cloud

3.2.2. ECMWF

Temperature profile

3.2.3. Coastline Map

Land or ocean flag.

3.2.4. Topographical Map

It provides altitude of surface above sea level to estimate the height of cloud above surface.

3.3 Input Variable Summary

(Generated by AIMS on 24 July 2007)

Dimensions Used

nray (typical value: 36383) Number of CPR rays in one orbit.
mod_1km (typical value: 15) 3 x 5 MODIS grid around CPR footprint.
Band_1KM_RefSB (typical value: 4) MODIS SW radiance channels
Band_1KM_Emissive (typical value: 11) MODIS LW radiance channels
nbin (typical value: 125) Number of CPR bins.

(1) Geodetic latitude of MODIS pixels

Name in file: MODIS_latitude **Range:** -90 to 90
Source: MODIS-AUX 007 **Missing value:** -999
Field type (in file): REAL(4) **Missing value operator:** ==
Field type (in algorithm): REAL(4) **Factor:** 1
Dimensions: mod_1km,nray **Offset:** 0
Units: degrees **MB:** 2.082

This array contains the vector of latitudes for the closest 15 pixels to the CloudSat CPR footprint in a 3x5 (across track x along track) grid.

(2) Geodetic longitude of MODIS pixels

Name in file: MODIS_longitude **Range:** -180 to 180
Source: MODIS-AUX 007 **Missing value:** -999
Field type (in file): REAL(4) **Missing value operator:** ==
Field type (in algorithm): REAL(4) **Factor:** 1
Dimensions: mod_1km,nray **Offset:** 0
Units: degrees **MB:** 2.082

This array contains the vector of longitudes for the closest 15 pixels to the CloudSat CPR footprint in a 3x5 (across track x along track) grid.

(3) MODIS Earth View 1KM Reflective Solar Bands Scaled Integers Subset

Name in file: EV_1KM_RefSB **Range:** 0 to 32767
Source: MODIS-AUX 007 **Missing value:** 32768
Field type (in file): UINT(2) **Missing value operator:** >=
Field type (in algorithm): UINT(2) **Factor:** 1
Dimensions: mod_1km,nray,Band_1KM_RefSB **Offset:** 0
Units: W/(m² str um) **MB:** 4.164

This data array contains radiances for MODIS band numbers 17-19 and 26. The full MODIS data has been subset to the closest 15 pixels around the CloudSat CPR footprint. More information can be obtained from the AN-MODIS ICD or from the MODIS web site at <http://mcstweb.gsfc.nasa.gov/product.html>.

(4) Radiance scales for EV_1KM_RefSB

Name in file: EV_1KM_RefSB_rad_scales **Range:** to
Source: MODIS-AUX 007 **Missing value:** -999
Field type (in file): REAL(4) **Missing value operator:** ==
Field type (in algorithm): REAL(4) **Factor:** 1
Dimensions: mod_granules,Band_1KM_RefSB **Offset:** 0
Units: -- **MB:** 0

Radiance scales needed to convert unscaled radiance data to scientific values.

(5) Radiance offsets for EV_1KM_RefSB

Name in file: EV_1KM_RefSB_rad_offsets **Range:** to
Source: MODIS-AUX 007 **Missing value:** -999

Field type (in file): REAL(4)	Missing value operator: ==
Field type (in algorithm): REAL(4)	Factor: 1
Dimensions: mod_granules,Band_1KM_RefSB	Offset: 0
Units: --	MB: 0

Radiance offsets needed to convert unscaled radiance data to scientific values.

(6) Reflectance scales for EV_1KM_RefSB

Name in file: EV_1KM_RefSB_ref_scales	Range: to
Source: MODIS-AUX 007	Missing value: -999
Field type (in file): REAL(4)	Missing value operator: ==
Field type (in algorithm): REAL(4)	Factor: 1
Dimensions: mod_granules,Band_1KM_RefSB	Offset: 0
Units: --	MB: 0

Reflectivity scales needed to convert unscaled radiance data to scientific values.

(7) Reflectance offsets for EV_1KM_RefSB

Name in file: EV_1KM_RefSB_ref_offsets	Range: to
Source: MODIS-AUX 007	Missing value: -999
Field type (in file): REAL(4)	Missing value operator: ==
Field type (in algorithm): REAL(4)	Factor: 1
Dimensions: mod_granules,Band_1KM_RefSB	Offset: 0
Units: --	MB: 0

Reflectivity offsets needed to convert unscaled radiance data to scientific values.

(8) MODIS Earth View 1KM Emissive Bands Scaled Integers Subset

Name in file: EV_1KM_Emissive	Range: 0 to 32767
Source: MODIS-AUX 007	Missing value: 32768
Field type (in file): UINT(2)	Missing value operator: >=
Field type (in algorithm): UINT(2)	Factor: 1
Dimensions: mod_1km,nray,Band_1KM_Emissive	Offset: 0
Units: W/(m2 str um)	MB: 11.45

This data array contains radiances for MODIS band numbers 20 and 27-36. The full MODIS data has been subset to the closest 15 pixels around the CloudSat CPR footprint. More information can be obtained from the AN-MODIS ICD or from the MODIS web site at <http://mctweb.gsfc.nasa.gov/product.html>.

(9) Radiance scales for EV_1KM_Emissive

Name in file: EV_1KM_Emissive_rad_scales	Range: to
Source: MODIS-AUX 007	Missing value: -999
Field type (in file): REAL(4)	Missing value operator: ==
Field type (in algorithm): REAL(4)	Factor: 1
Dimensions: mod_granules,Band_1KM_Emissive	Offset: 0
Units: --	MB: 0.001

Radiance scales needed to convert unscaled radiance data to scientific values.

(10) Radiance offsets for EV_1KM_Emissive

Name in file: EV_1KM_Emissive_rad_offsets	Range: to
Source: MODIS-AUX 007	Missing value: -999
Field type (in file): REAL(4)	Missing value operator: ==
Field type (in algorithm): REAL(4)	Factor: 1
Dimensions: mod_granules,Band_1KM_Emissive	Offset: 0
Units: --	MB: 0.001

Radiance offsets needed to convert unscaled radiance data to scientific values.

(11) Seconds since the start of the granule.

Name in file: Profile_time	Range: 0 to 6000
Source: 2B-GEOPROF 011	Missing value:
Field type (in file): REAL(4)	Missing value operator:
Field type (in algorithm): REAL(4)	Factor: 1

(18) Data status flags

Name in file: Data_status **Range:** 0 to 127
Source: 2B-GEOPROF 011 **Missing value:**
Field type (in file): UINT(1) **Missing value operator:**
Field type (in algorithm): INT(2) **Factor:** 1
Dimensions: nray **Offset:** 0
Units: -- **MB:** 0.035

This is a bit field that contains data status flags:

Bit 0: missing frame (0=false, 1=true)
Bit 1: SOH missing (0=false, 1=true)
Bit 2: GPS data valid (0=false, 1=true)
Bit 3: 1 PPS lost (0=false, 1=true)
Bit 4: Star tracker 1 (0=off, 1=on)
Bit 5: Star tracker 2 (0=off, 1=on)
Bit 6: Coast (0=false, 1=true)
Bit 7: NISC (0=false, 1=true)

(19) Land Sea Flag

Name in file: Navigation_land_sea_flag **Range:** 1 to 3
Source: 2B-GEOPROF 011 **Missing value:**
Field type (in file): UINT(1) **Missing value operator:**
Field type (in algorithm): INT(2) **Factor:** 1
Dimensions: nray **Offset:** 0
Units: -- **MB:** 0.035

Flag indicating whether spacecraft is over land or sea:

1 = land
2 = ocean
3 = coast

(20) Radar Reflectivity Factor

Name in file: Radar_Reflectivity **Range:** -40 to 50
Source: 2B-GEOPROF 011 **Missing value:** -88.88
Field type (in file): INT(2) **Missing value operator:** ==
Field type (in algorithm): REAL(4) **Factor:** 0.01
Dimensions: nbin,nray **Offset:** 0
Units: dBZe **MB:** 8.674

Radar reflectivity factor Ze is calculated with the echo power and other input data as described in Li and Durden (2001)

(21) CPR Cloud Mask

Name in file: CPR_Cloud_mask **Range:** 0 to 40
Source: 2B-GEOPROF 011 **Missing value:** -9
Field type (in file): INT(1) **Missing value operator:** ==
Field type (in algorithm): INT(1) **Factor:** 1
Dimensions: nbin,nray **Offset:** 0
Units: **MB:** 4.337

Each CPR resolution volume is assigned 1 bit mask value:

0 = No cloud detected
1 = likely bad data
5 = likely ground clutter

5-10 = week detection found using along track integration.
20 to 40 = Cloud detected .. increasing values represents clouds with lower chance of a being a false detection.

(22) Height of range bin in Reflectivity/Cloud Mask above reference surface (~ mean sea level).

Name in file: Height	Range: -5000 to 30000
Source: 2B-GEOPROF 011	Missing value: -9999
Field type (in file): INT(2)	Missing value operator: ==
Field type (in algorithm): INT(2)	Factor: 1
Dimensions: nbin,nray	Offset: 0
Units: m	MB: 8.674

Height of the radar range bins in meters above mean sea level.

(23) Location of Surface Bin as determined by 1B CPR algorithm. The value here is shifted (as Height).

Name in file: SurfaceHeightBin	Range: 1 to 125
Source: 2B-GEOPROF 011	Missing value: -1
Field type (in file): INT(1)	Missing value operator: ==
Field type (in algorithm): INT(1)	Factor: 1
Dimensions: nray	Offset: 0
Units:	MB: 0.035

Location of Surface Bin as determined by 1B CPR algorithm. The value here is shifted (as is the Height matrix) so bins in neighboring rays are about the same height.

(24) MODIS scene characterizations

Name in file: MODIS_scene_char	Range: 0 to 9
Source: 2B-GEOPROF 011	Missing value: -9
Field type (in file): INT(1)	Missing value operator: ==
Field type (in algorithm): INT(1)	Factor: 1
Dimensions: nray	Offset: 0
Units:	MB: 0.035

This data includes MODIS pixel cloudiness characterization using cloudmask bit tests. See Table 3 in GEOPROF documentation for a detailed specification.

(25) MODIS scene variability

Name in file: MODIS_scene_var	Range: 0 to 5
Source: 2B-GEOPROF 011	Missing value: -9
Field type (in file): INT(1)	Missing value operator: ==
Field type (in algorithm): INT(1)	Factor: 1
Dimensions: nray	Offset: 0
Units:	MB: 0.035

MODIS scene variability -variability of classification assigned to the 1 km MODIS pixels that compose the CloudSat footprint and immediately adjacent region. See Table 5 for a detail specification.

(26) MODIS 250m Cloud Fraction

Name in file: MODIS_Cloud_Fraction	Range: 0 to 100
Source: 2B-GEOPROF 011	Missing value: -99
Field type (in file): INT(1)	Missing value operator: ==
Field type (in algorithm): INT(1)	Factor: 1
Dimensions: nray	Offset: 0
Units:	MB: 0.035

MODIS 250m cloud fraction included cloud fraction calculated with MODIS 250m pixels.

(27) Atmospheric pressure

Name in file: Pressure	Range: to
-------------------------------	------------------

Source: ECMWF-AUX 008
Field type (in file): REAL(4)
Field type (in algorithm): REAL(4)
Dimensions: nbin,nray
Units: Pa

(28) Temperature

Name in file: Temperature
Source: ECMWF-AUX 008
Field type (in file): REAL(4)
Field type (in algorithm): REAL(4)
Dimensions: nbin,nray
Units: K

(29) Specific humidity

Name in file: Specific_humidity
Source: ECMWF-AUX 008
Field type (in file): REAL(4)
Field type (in algorithm): REAL(4)
Dimensions: nbin,nray
Units: kg/kg

(30) Surface pressure

Name in file: Surface_pressure
Source: ECMWF-AUX 008
Field type (in file): REAL(4)
Field type (in algorithm): REAL(4)
Dimensions: nray
Units: Pa

(31) Skin temperature

Name in file: Skin_temperature
Source: ECMWF-AUX 008
Field type (in file): REAL(4)
Field type (in algorithm): REAL(4)
Dimensions: nray
Units: K

Skin temperature.

(32) Two-meter temperature

Name in file: Temperature_2m
Source: ECMWF-AUX 008
Field type (in file): REAL(4)
Field type (in algorithm): REAL(4)
Dimensions: nray
Units: K

Two-meter temperature.

Missing value: -999
Missing value operator: ==
Factor: 1
Offset: 0
MB: 17.349

Range: to
Missing value: -999
Missing value operator: ==
Factor: 1
Offset: 0
MB: 17.349

Range: to
Missing value: -999
Missing value operator: ==
Factor: 1
Offset: 0
MB: 17.349

Range: to
Missing value: -999
Missing value operator: ==
Factor: 1
Offset: 0
MB: 0.139

Range: to
Missing value: -999
Missing value operator: ==
Factor: 1
Offset: 0
MB: 0.139

Range: to
Missing value: -999
Missing value operator: ==
Factor: 1
Offset: 0
MB: 0.139

3.4. Control and Calibration

No control and calibration are necessary for this algorithm.

4. Algorithm Summary

First algorithm performs clustering analysis to group individual cloud profile into a cloud cluster, then applies rules and classification methods to classify it into different cloud types. The details of the algorithm are also discussed here.

4.1. Cloud clustering analysis

Cloud layer: CloudSat bins with significant cloud mask values (≥ 30) and vertically connected are regarded as a cloud layer.

Cloud Cluster: a group of cloud layers horizontally connected with a similar vertical coverage is analyzed together as a cloud cluster.

Because of the strong variability of clouds, it is difficult to apply a classification algorithm directly to an individual radar profile. Different types of clouds have different horizontal and vertical extents. The cloud clustering analysis provides cloud horizontal and vertical extent features. Cloud layer structure is first determined by using bins with significant cloud mask values (≥ 30). Then we cooperate bins with mask values between 20 and 30 into the identify layer structure. The bins connected to first layer based are included as the first layer and the bins directly above top layer are regarded part of top layer. For the bins between two layers will be treated according to their connections to the exiting layers. If they only connect lower or higher layer, they will be included to corresponding connected layer. If they fill the gap between two layers, we decide whether to combine two layers into one layer or include them into one layer and keep two layer structure based on signal intensities and height of existing layers. If these weaker bins form an isolated layer between two existing layers, they will not be included for analysis. If there is no cloud layer identified with mask values ≥ 30 , new layer structure is simply determined based on bins with mask values between 20 and 30.

For some cloud types, such as Cu and Sc, horizontal extent of a cloud element may be small. Therefore, it is necessary to set a minimum horizontal extent for a cloud cluster to capture the inhomogeneity of clouds. Currently, 30 km horizontally is search for broken clouds normally. A search for a cloud cluster is terminated when a large change in cloud vertical or horizontal structures is detected, such as, cloud evolve from anvil to deep convective core, cloud base change from low level to middle level or from middle level to low or high level or from high to middle, and sharp cloud thickness change. A

CloudSat granule may be divided into a different number of cloud clusters varying with cloud type presented in the granule.

The following variables are calculated for each cluster and used for cloud type classification:

Maxtop: maximum top height for the cloud cluster, km, AGL
meantop: mean cloud top height, km,AGL
devtop: Standard deviation of cloud top height
meantopT: mean cloud top temperature
mintopT: lowest cloud top temperature
meanbase: mean cloud base height, km, AGL
devbase: Standard deviation of cloud base height
meanbaseT: mean cloud base temperature, degree
minbase: lowest cloud base for the cloud cluster
Max10db_H: Maximum 10 dBZ height for the cloud cluster, AGL
meanDz: mean cloud thickness, km
maxDz: maximum cloud thickness
meanlat: the mean latitude for the cloud cluster
meanze: mean maximum Z_e (maximum Z_e is calculated for each profile), dBZ
devZe: standard deviation of maximum Z_e
maxZeV: maximum Z_e value of the cloud cluster
meanHeight: mean maximum Z_e height
meantemp: mean temperature at the maximum Z_e height
length: Cluster horizontal length, km
Index_precipitation: number of precipitating cloud profiles
Cloud_F: Cloud fraction
Inhomo: Cloud inhomogeneity measured by standard deviation of maximum Z_e divided by mean maximum Z_e both in unit of mm^6/m^3

4.2. The flowchart of cloud scenario classification

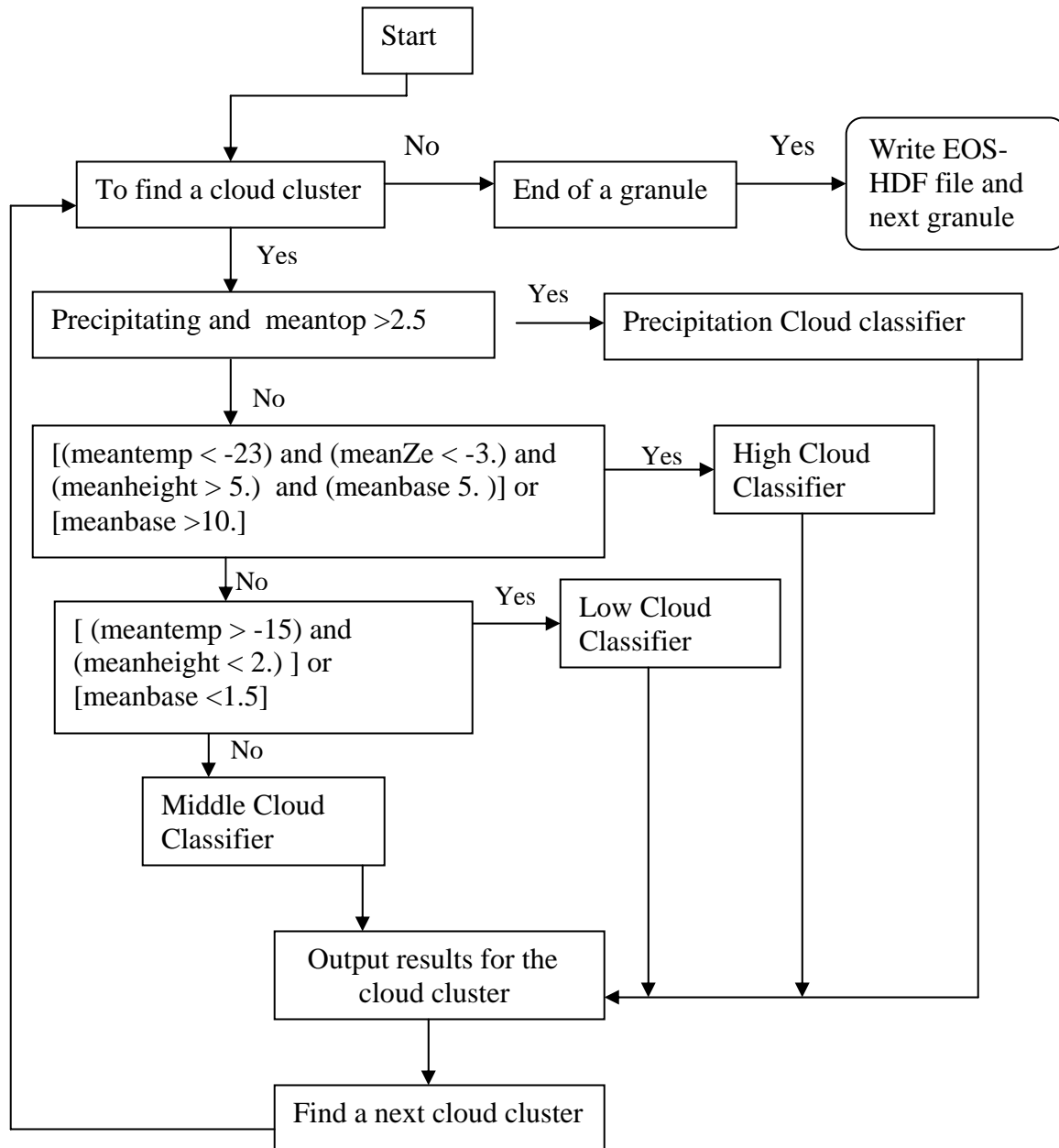


Figure 4: The high level flowchart of cloud scenario classification algorithm

Figure 4 shows the general structure of CloudSat scenario classification algorithm. Once a cloud cluster is found, cloud height, temperature, and maximum Z_e , as well as the occurrence of precipitation apparently reaching the surface, are determined. The clouds with precipitation will be classified as either Ns, St, Sc, Cu Ac, or deep convective according to their vertical and horizontal extent, maximum Z_e values and height,

horizontal extent, and strength of the precipitation [Wang and Sassen, 2001]. A non-precipitating cloud cluster is passed to a high, middle, or low classifier according to its mean cloud height and temperature, cloud base and top height (and its variability), and Z_e magnitude and spatial variability. More detail information for the four classifier boxes in this flowchart is presented in section 4.4.

4.3. Precipitation Identification

Precipitation identification is an important step in the classification scheme. Here we summarize the principles used in the algorithm. Precipitation has larger size comparing with cloud particles; therefore the reflectivity factor of precipitation is stronger than that from clouds. However, space-borne cloud radar does not always detect strong signal from precipitation because of attenuation of clouds and precipitation itself. In the case of strong attenuation of clouds and precipitation, the signal from surface will also be attenuated. Figure 5 gives an example from airborne 94 GHz cloud radar measurements 24 June 1996. The attenuation of cloud and precipitation can reduce surface signal up to 30 dBZ.

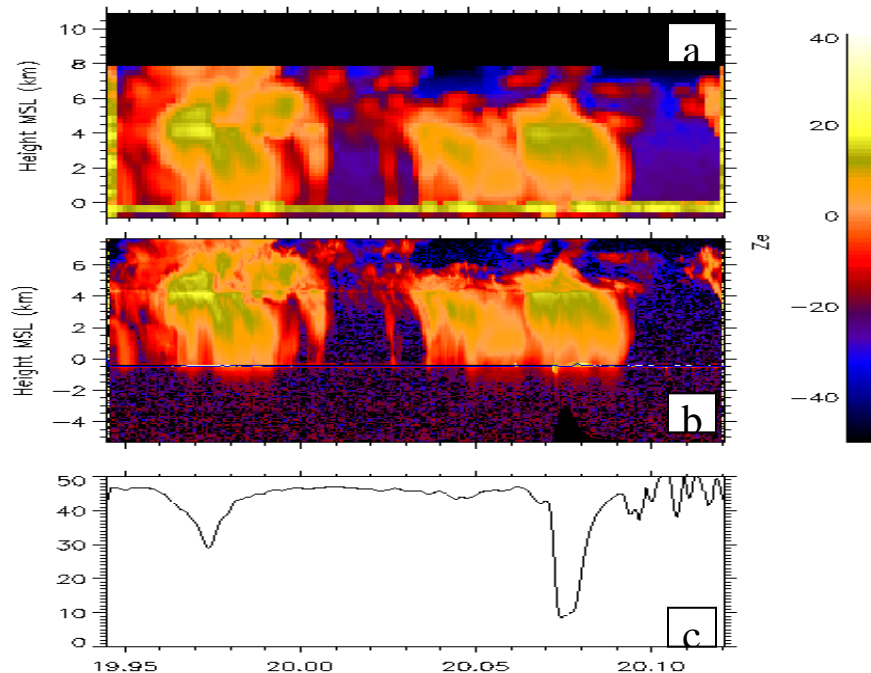


Figure 5. Example of airborne 94 GHz cloud radar measurements (b) on 24 June 1996. a) shows simulated CloudSat radar signal according to the measurements shown in b), and c) shows the surface return.

Therefore, we combine the maximum reflectivity in lower radar gate and attenuation of cloud and precipitation to identify the occurrence of precipitation. Figure 6 shows the frequency distribution of the maximum radar reflectivity factor within 2 km above surface from MMCR measurements at different CART sites and airborne 94 GHz cloud radar measurements. Each CART site result generated from more than one year data and airborne radar data is from four field experiments (<http://abyss.ecs.umass.edu/acr-web/data.html>). There are obvious multi-mode distributions except NSA data, which reflects the contributions of clouds, drizzle and precipitation. There are local minimums between -10 and 0 dBZ, and vary from site to site. The existence of local minimums indicates that we can select a threshold to distinguish precipitation from cloud though it is not accurate every time. Boundary cloud from NSA site is different than other site due to relative cold environment.

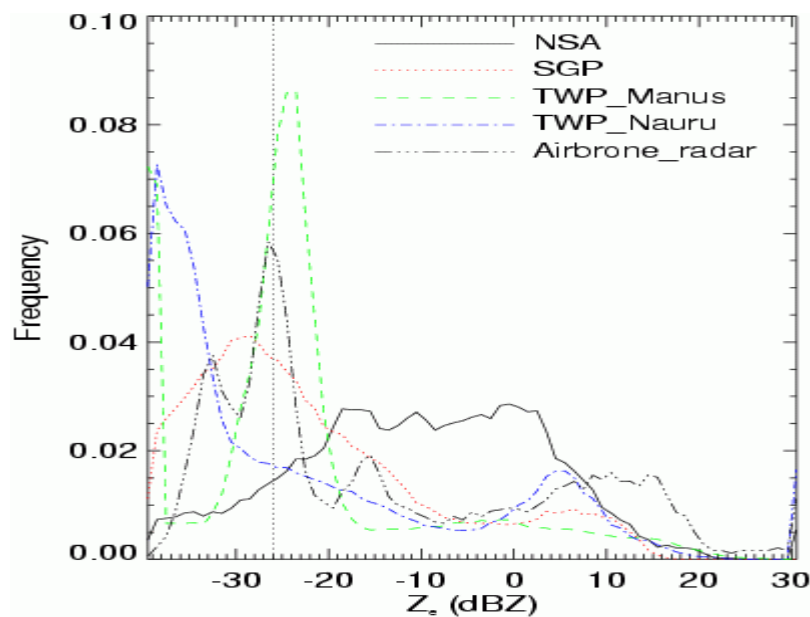


Figure 6: The frequency distribution of the maximum radar reflectivity factor within 2 km above surface from MMCR measurements at SGP, NSA and TWP sits and airborne cloud radar measurements. The vertical dashed line indicates the -26 dBZ.

One possible challenge to use the maximum radar reflectivity in low radar bins to identify precipitation is the effect of surface return signal and limited vertical resolution of CloudSat. Figure 7 shows an example of airborne cloud radar measurements of boundary clouds. The simulated CloudSat signals indicate that the surface signal makes cloud detection and precipitation identification in first two bins above surface difficult. CloudSat data indicated that the closest four bins above surface are contaminated by surface cluster although bin three and four above surface could be recovered under favorable conditions. Currently, CloudSat has implemented an approach to recover these bins when it is possible.

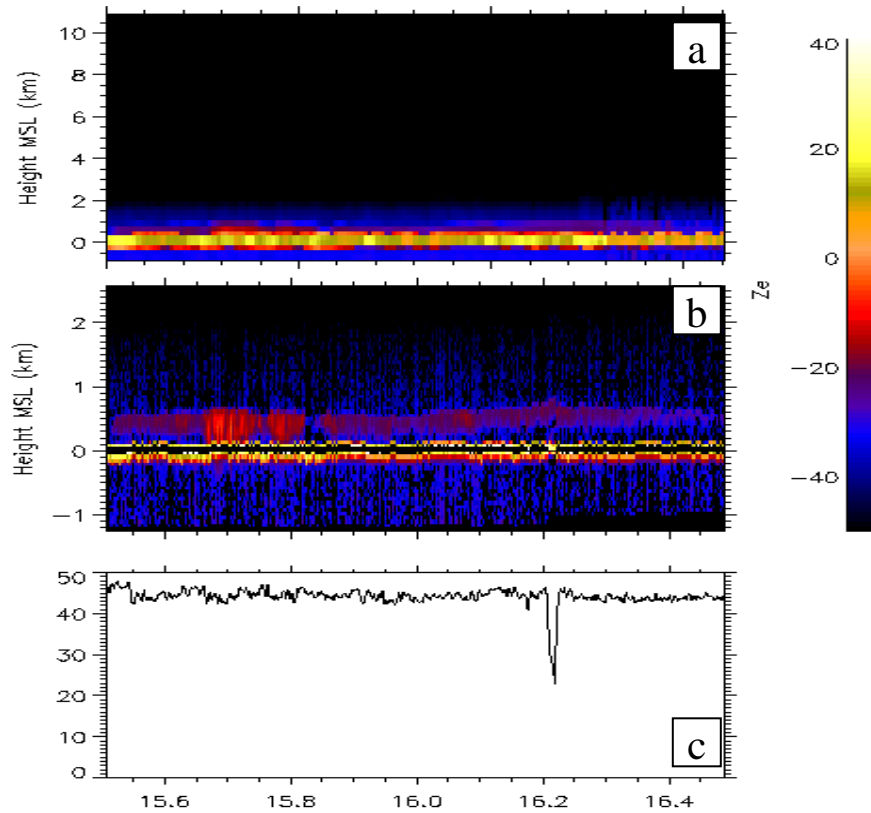


Figure 7. Same as Fig.5 expect for 3 July, 1999

To study the reliability of using CloudSat signal around 1 km above surface to detect occurrence of precipitation at surface, the radar signal correlation between 1 km and near surface (~ 100 m) are presented in Fig. 8 based on ARM observations at tropical (TWP), midlatitude (SGP), and Polar (NSA) regions. It is clear that radar signal at these two levels are highly correlated though there are slightly differences among sites. For example, when signals at 1 km reach 0 dBZ, near surface signals are expected higher than -10 dBZ at $\sim 90\%$ of time over the TWP and NSA sites. Compared with TWP and NSA sites, the SGP site has $\sim 10\%$ higher chance to observe smaller Z_e than -10 dBZ based on Fig. 8. The coarse resolution of CloudSat is supposed to make situations better.

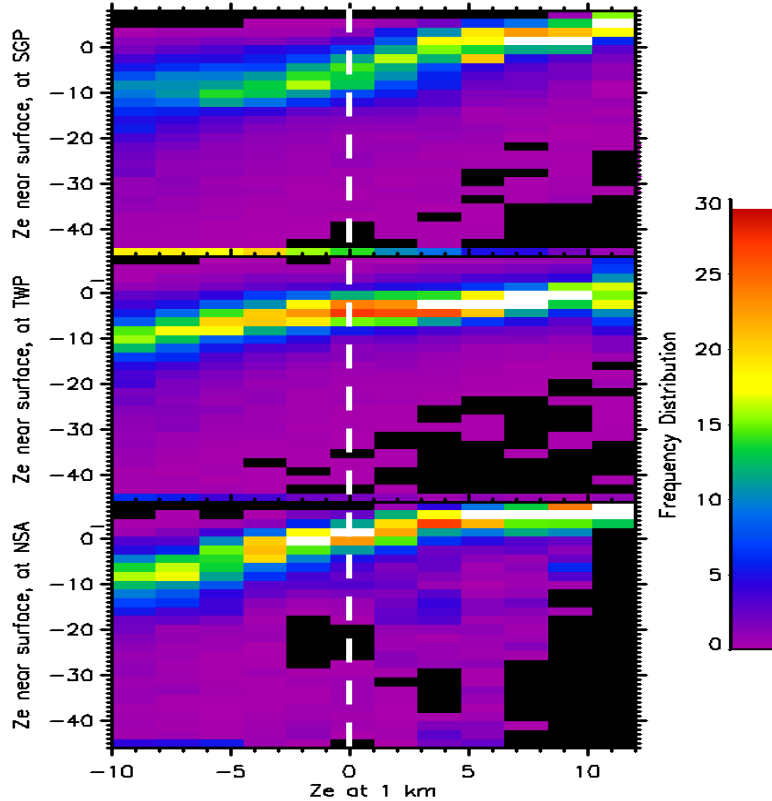


Figure 8. The correlation of near surface radar signals with signals at 1 km based on ARM surface observations at three different climate regions

Based on above discussion, the following temperature dependent threshold (see Fig. 9) is selected to detect the occurrence of precipitation based on first non-surface contaminated bins (3 to 5 bins above surface). To cover heavy precipitation cases, surface signal intensities are further evaluated to find strong attenuation period due to precipitation. Surface signals are determined by many factors and surface type is a main one. Over water, surface signal is mainly controlled by wind speed (Haynes and Stephens 2007). Over land, surface signals are affected by soil type and moisture and vegetation. Figure 10 presents the frequency distributions of CloudSat surface bin signals over land and ocean, respectively. It is clear that the distributions over ice and ocean are narrower than land. Figure 10 provides a general guidance on how to set up thresholds to use surface signals to detect strong attenuation in CloudSat signals due to precipitation. First, it is hard to find a single threshold for global application. Therefore, regional surface reference signals are determined by finding the minimum surface signal under clear or mid- or high-level cloud conditions within 30 km of the profiles to be analyzed. If there is no clear or mid- or high-level cloud condition found within 30 km, the reference signal for the nearby one will be used. The regional reference signal minus 6 is used as a threshold to identify profiles with strong attenuation near surface. To minimize the false detection, maximum Z_e within 25 bins above surface also require large than selected thresholds depending on surface signals.

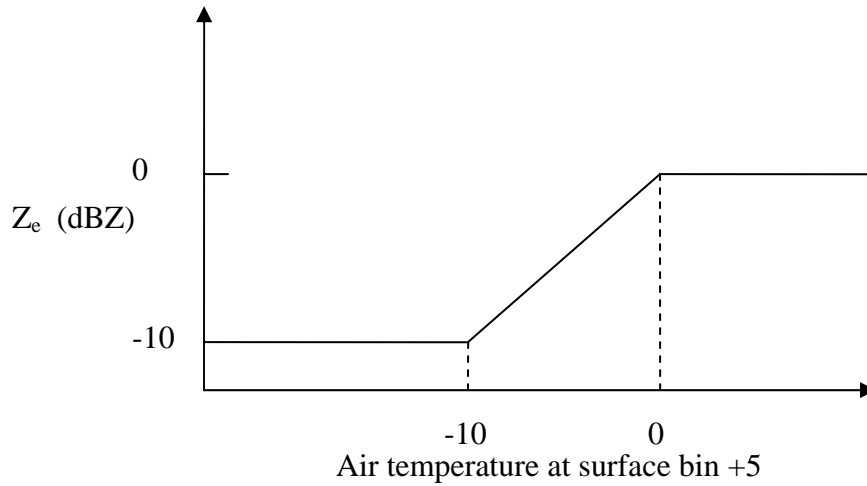


Figure 9, Z_e threshold for precipitation detection based on near surface CloudSat signal intensity and air temperature.

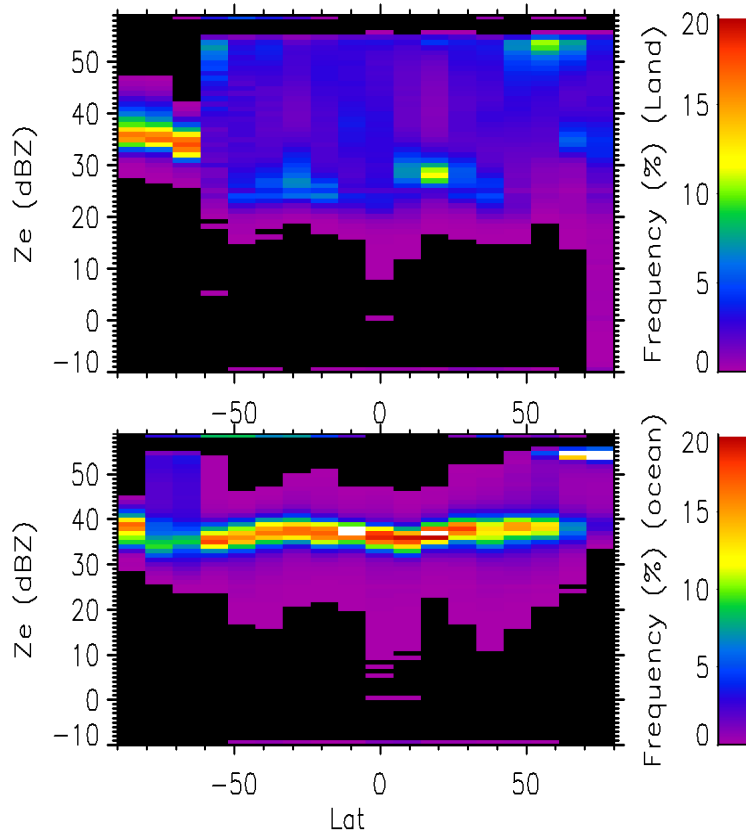


Figure 10, Surface maximum reflectivity distribution as a function latitude based on one month CloudSat data: top for measurements over land and bottom for measurements over ocean. High occurrence regions represent surface return under clear, non-precipitation, or weak precipitation conditions.

The phase of precipitation can be approximately discriminated from temperature profile and the occurrence of bright band in radar signal. Figure 11 shows the comparison of two different phase precipitation and related temperature profiles. If the bright band is identified and/or the temperature near surface is at least warmer than 2 degrees the precipitation is regarded as liquid. Otherwise, the precipitation is labeled as solid precipitation.

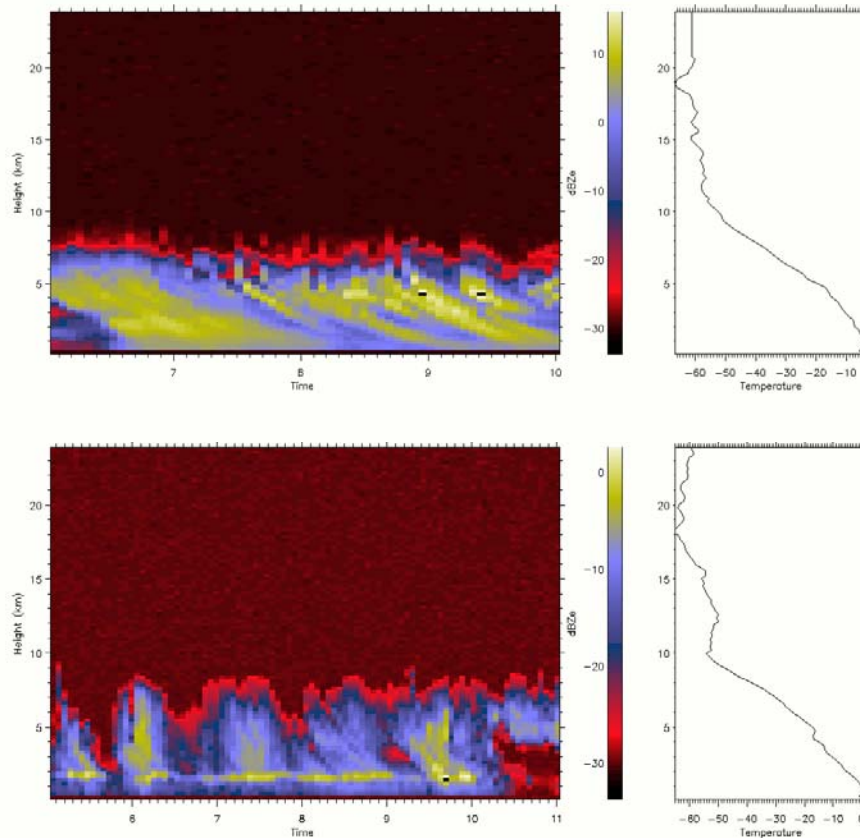


Figure 11 shows the comparison of two different phase precipitation and related temperature profiles. Top: solid precipitation and temperature below zero degree; and bottom liquid precipitation with bright band.

After precipitation identification, first cloud layer above surface will be analyzed for possible occurrence of drizzle. The most reliable way to identify drizzle in boundary layer clouds is to use vertical Z_e profile. When no drizzle presented, Z_e values increase with height; when drizzle presented Z_e values is normally decrease with height. Unfortunately, we can not apply this to CloudSat data for drizzle identification due to the 500 m vertical resolution of CloudSat data (over sampled at 240 m vertical resolution). Therefore, we have to rely on the magnitude of CloudSat Z_e measurements only.

There are different thresholds (ranging from -20 to -10 dB) suggested for indicating drizzle occurrence based on ground-based or airborne measurements from different regions (Wang and Geerts, 2003; Matrosov et al. 2004). However, we have to consider the vertical resolution differences between CloudSat and group-based or airborne radar systems if we want to use any suggested thresholds. To select a proper threshold, we study the maximum Z_e distributions for marine clouds with cloud top below 3.5 km, which are presented in Fig. 12. It is clear that maximum Z_e show a multi-mode distribution which represents contributions from cloud, drizzle, and precipitation. Between -25 and -10 dBZ, there is a local minimum around ~ -18 dBZ, which only show a slight dependency on regions and seasons. Based on these statistics, -18 dBZ is selected to detect possible drizzle occurrence based on maximum Z_e for the boundary layer clouds.

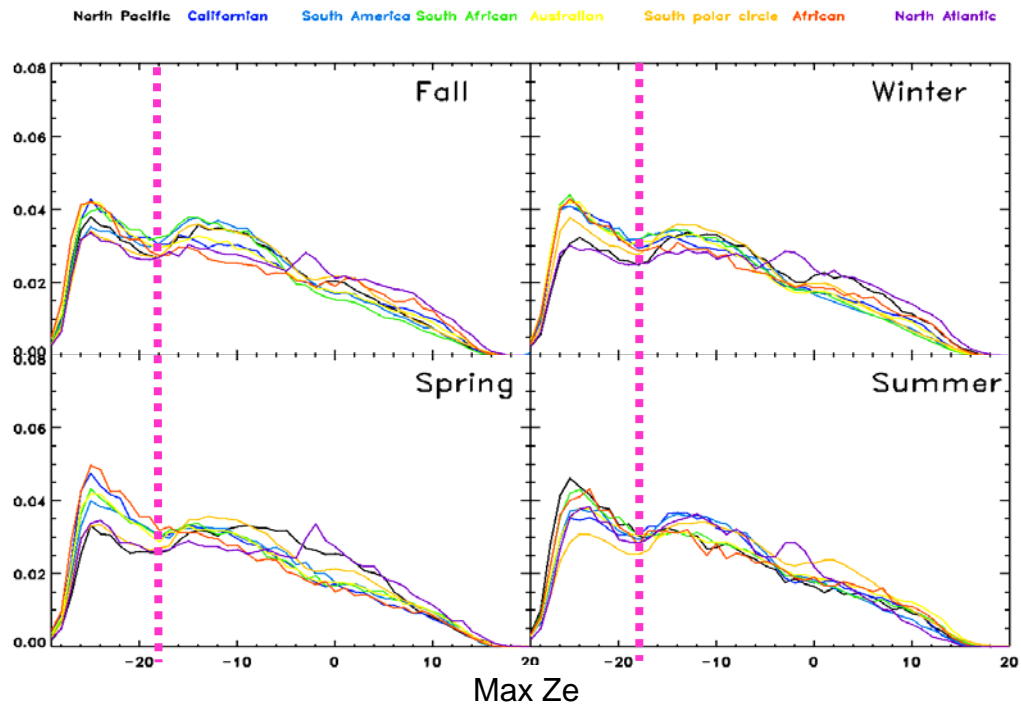


Figure 12. Maximum Z_e distribution for marine clouds with cloud top below 3.5 km over 8 Sc cloud occurrence regions (color coded). The Z_e values presented here are non-attenuation corrected CloudSat measurements from June 2006 to April 2007.

4.4. Role-based Cloud Classification

The challenge part of the role-based cloud classification is selected threshold values for different parameters to design a decision tree. The flowchart given in Fig. 4 represents high-level decision tree structure. The logic in each box is turned based on CloudSat data, which is more complex than roles given in table 2. With the vertical structure of clouds identified, it is relatively straightforward to put a cloud layer into low, middle, or high cloud levels [WMO, 1965]. However, precipitation makes it impossible to infer

cloud base heights of precipitating clouds, which complex situation slightly. Typical CloudSat images for different cloud types are showed in Fig. 13. It is clear that there are distinguishable features among them. The key of the algorithm is to find effective ways to distinguish cloud types in the same level and to consider their differences over different latitudes or seasons.

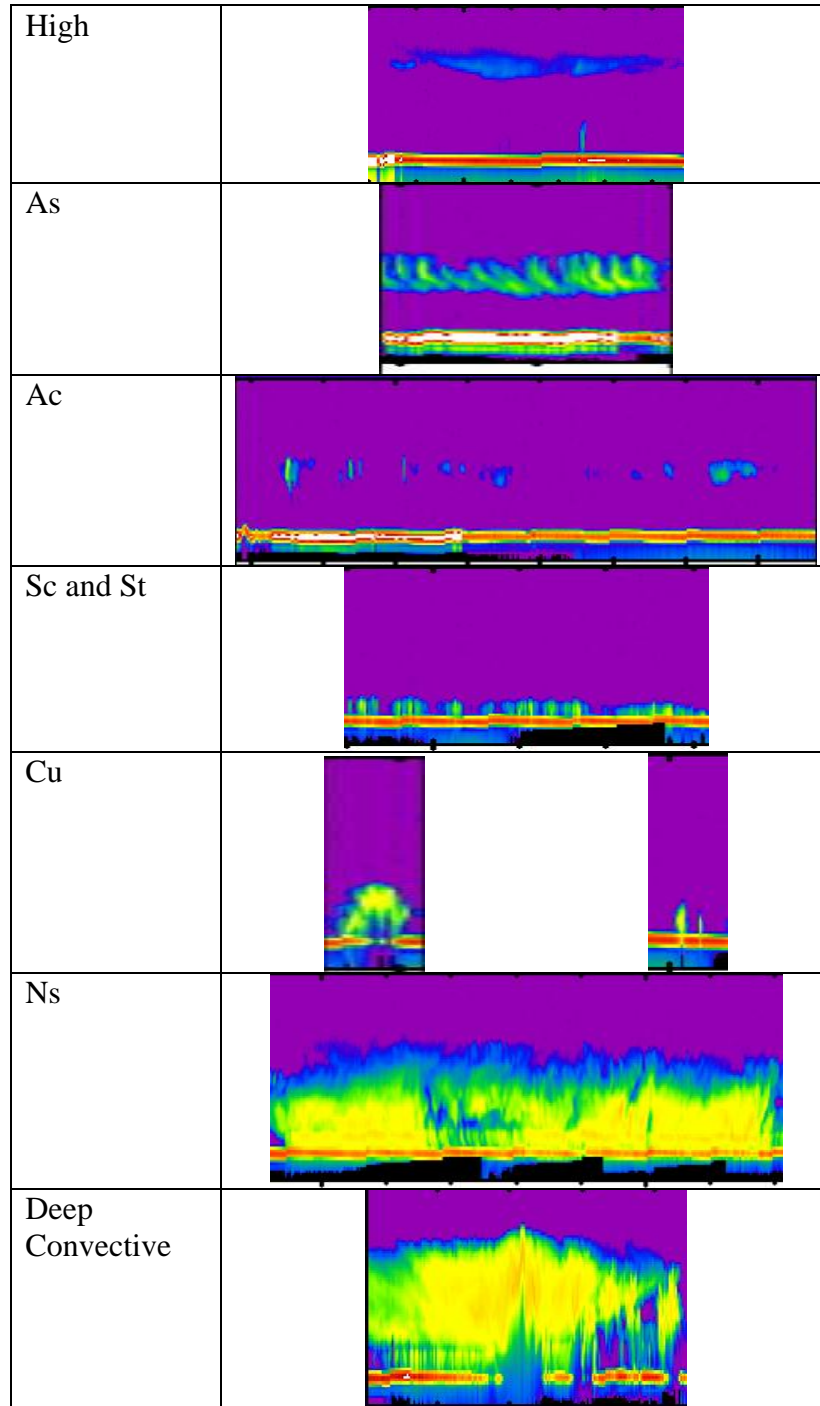


Figure 13. Typical examples of different cloud types observed by CloudSat. Horizontal axis represents distance along CloudSat track, and vertical axis

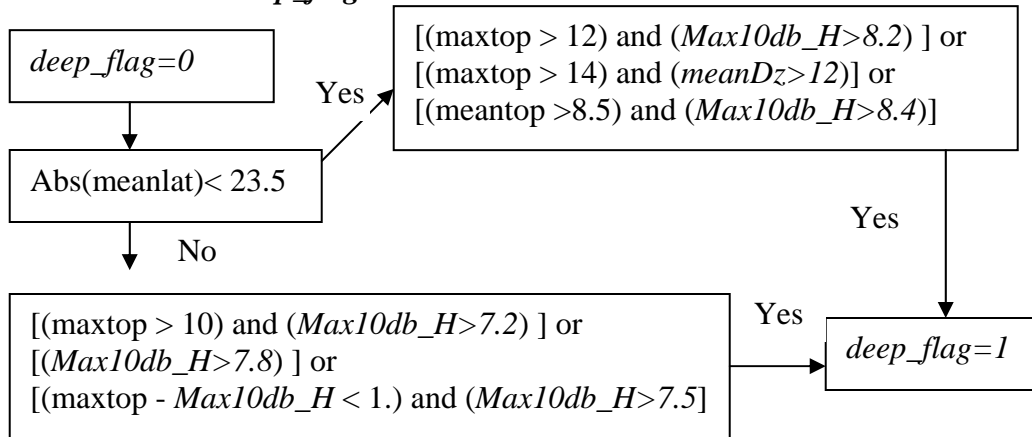
represents cloud altitude. Surface height is indicated by strong signals (red or white colors) except regions strongly attenuated by precipitation.

Middle level clouds include Ac and As. The main difference between them is cloud composition. As is mainly composed ice crystals though water droplets could be present. On the other hand, Ac is mainly composed water droplets though ice crystals could be present and fall as virga. This microphysical property difference results in a significant difference in Z_e [Wang and Sassen, 2001], which helps to separate these two types of clouds.

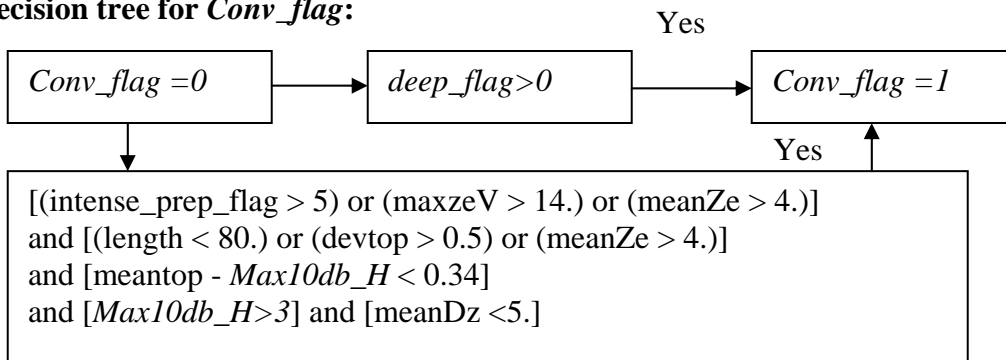
Both Ns and deep convective clouds could extend from near the surface to the upper troposphere in term of hydrometer profiles from radar measurements. The main difference between these two main precipitating clouds is their precipitation intensity. Compared with Ns clouds, deep convective clouds generally produce heavier precipitation, which is reflected by weak surface returns due to the rainfall attenuation at 94 GHz. Another difference between them is their formation mechanisms. Ns is most often formed as a result of the slow ascent of extensive layers. On the other hand, deep convective clouds are normally associated with strong updrafts during formation. Therefore, hydrometer vertical distributions are different between them, and deep convective clouds usually have stronger signals near cloud top than Ns clouds. Cumulus congestus could also produce strong precipitation. They are separated from Ns by their horizontal length scale and whether convective cells are present. The difference between cumulus congestus and deep convective clouds is mainly based cloud top height.

If a cloud cluster including a precipitating profile and mean cloud top height higher than 2.5 km, this cloud cluster will be directed into precipitating cloud classifier. First, precipitation intensity is analyzed to set values for *Intense_prep_flag* and *Very_intense_prep_flag* based on surface signals. If the surface signal of a profile is smaller than 20 dBZ over ocean or 10 dBZ over land, *Intense_prep_flag* will be increased by 1. If surface signal is smaller than -10 dBZ, *Very_intense_prep_flag* will be increased by 1. The next task is to judge whether the cluster is Ac clouds, which is characterized by *flat* middle level top (between 2.9 and 7 km), light precipitation (*Intense_prep_flag* < 1), large cloud base change, and small mean maximum Z_e (< -6 dB, maximum Z_e is calculated for each profile). If the precipitating cloud cluster is not a Ac, the cluster will be analyzed to decide whether it is need to separate into before, after, and during precipitation periods. The reason for this step is that a precipitating cluster could include a large portion non-precipitating cloud profiles. Before and after precipitation periods will be redirected to low, middle, or high cloud classifier according to cloud base and top heights. The decision tree for the precipitation period is given in Fig. 14. To better separate deep convective clouds and Ns and to identify well developed Cu congestus, two variables, *deep_flag* and *Conv_flag*, are assigned to have value 0 or 1 based on the following logics to characterize the vertical structure of Z_e .

Decision tree for *deep_flag*:



Decision tree for *Conv_flag*:



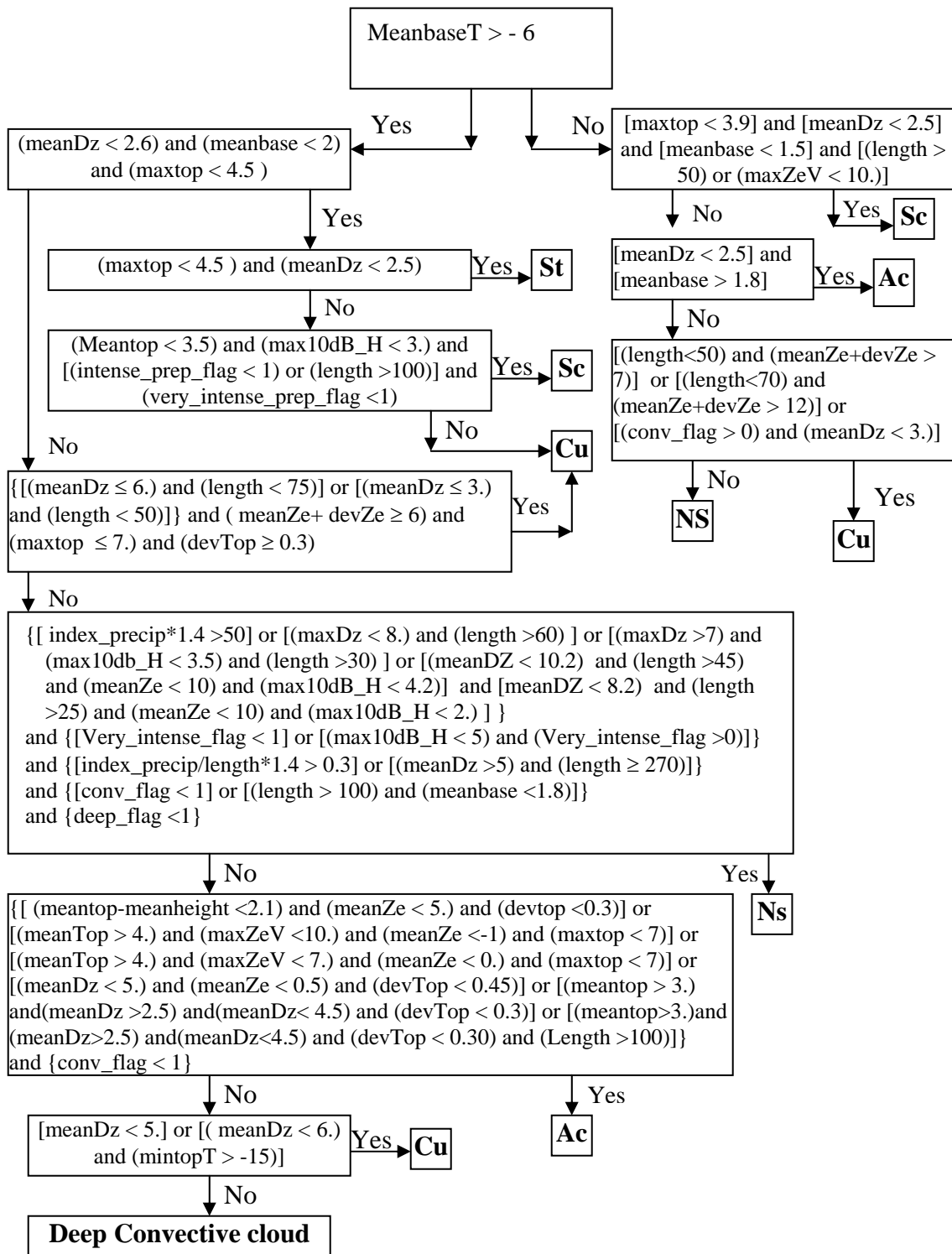
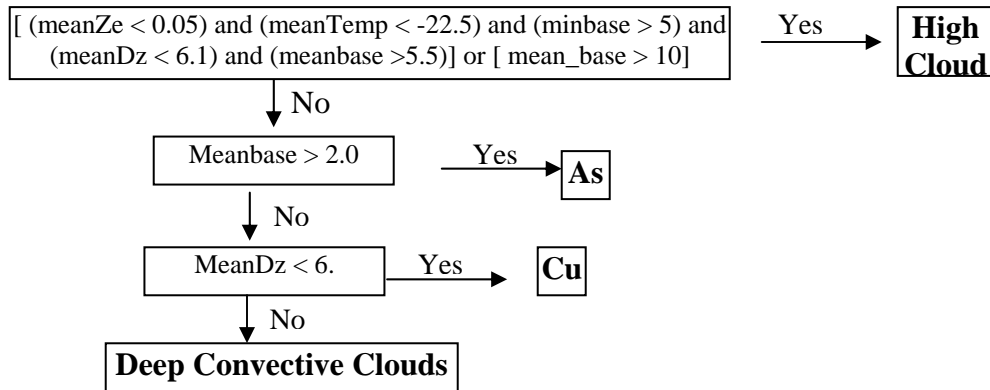


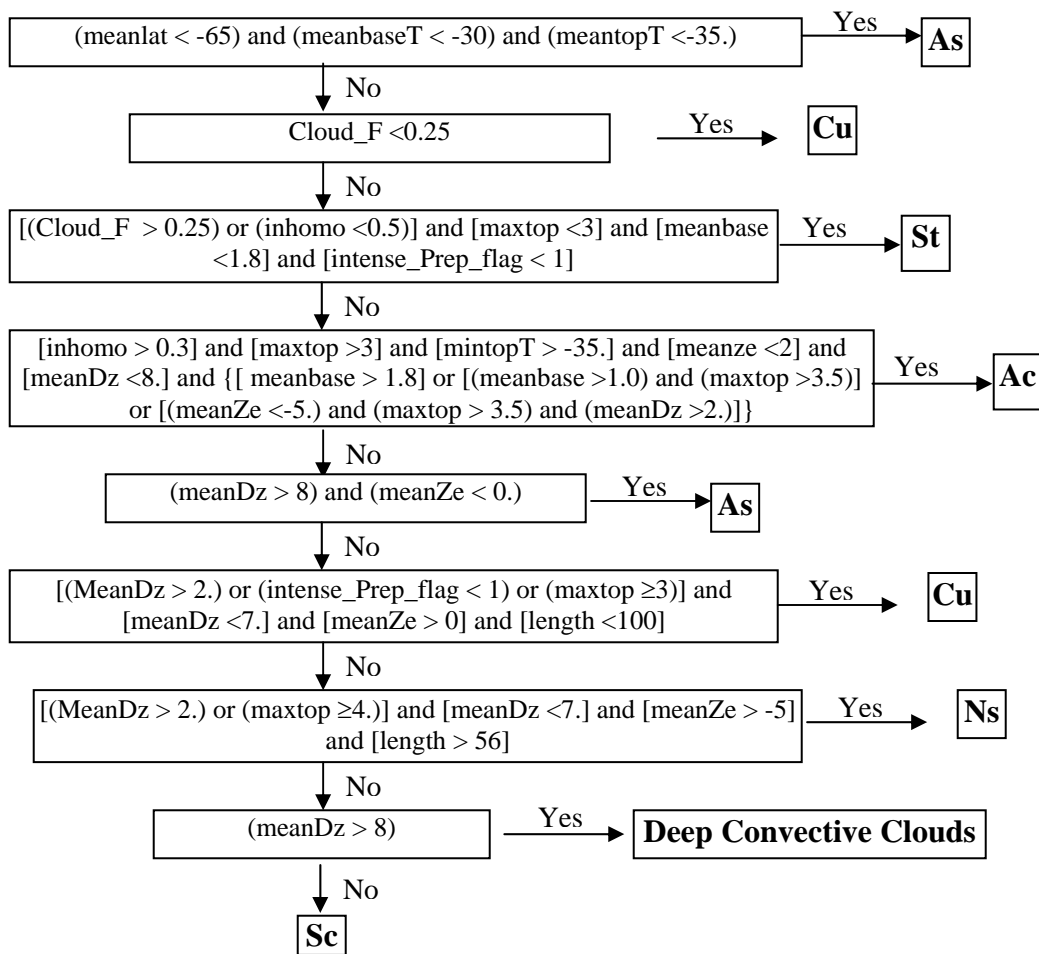
Figure 14: The decision tree for precipitating cloud classification.

The decision trees for low, middle, and high cloud classifier are given below.

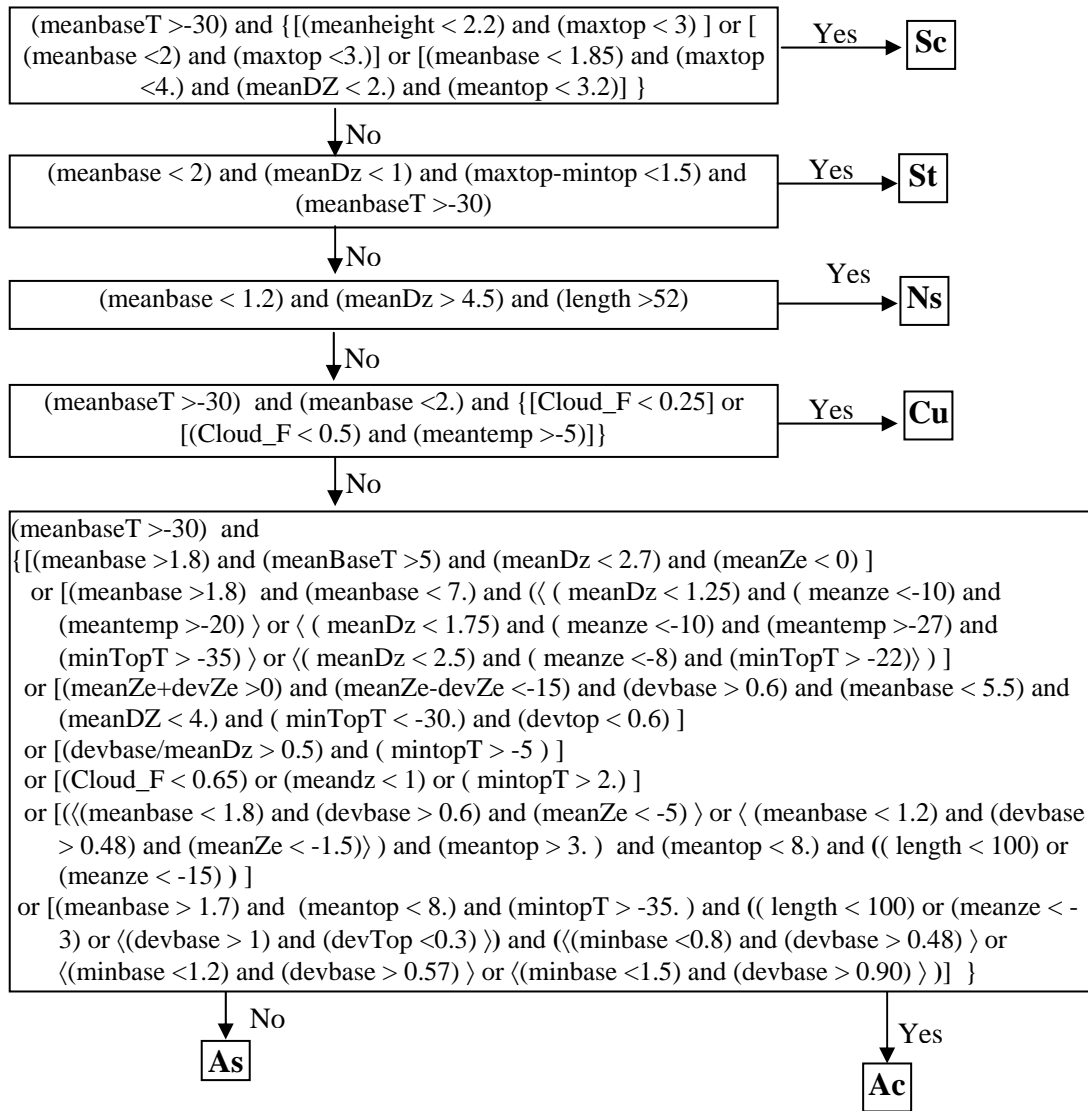
The decision tree of high cloud classifier:



The decision tree of low cloud classifier:



The decision tree of middle cloud classifier:



An example of results is given in Figure 15. The flight track of CloudSat is depicted on the merged satellite IR image between 60 S and 60N in Fig. 15a. The southern end of the track corresponds to the left edges of Fig. 15b-e. The calibrated CPR Ze is presented in Fig. 15d (in terms of $\text{dBZ}=10 \log Ze$), which together with the cloud mask (Fig. 15c) are the basic inputs of the algorithm. Figure 15e presents the ECMWF temperature profiles under the CloudSat ground track, which are used to determine cloud temperature. The corresponding cloud type classification results are presented in Fig. 15b. As indicated in Fig. 15a, CloudSat fortuitously flew directly over hurricane *Ileana*, which is identified by the deep convective clouds in Fig. 15b.

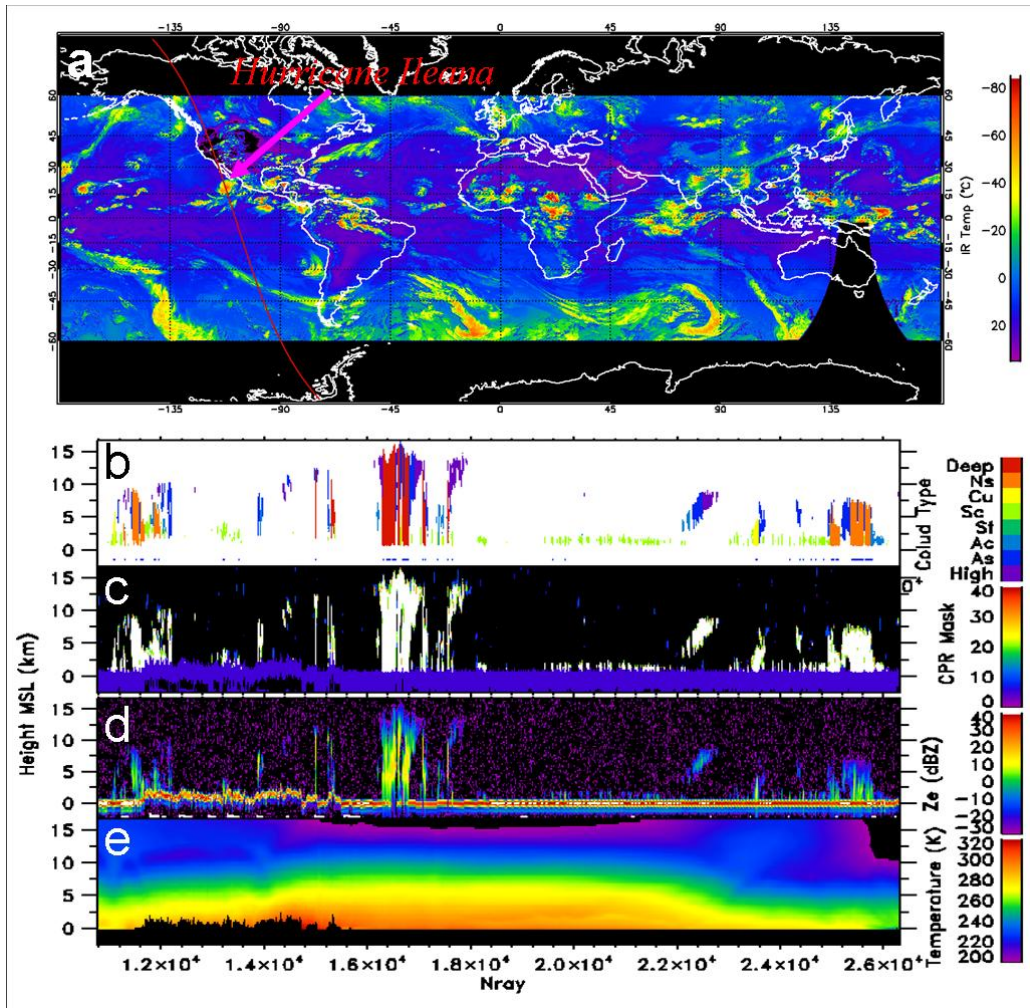
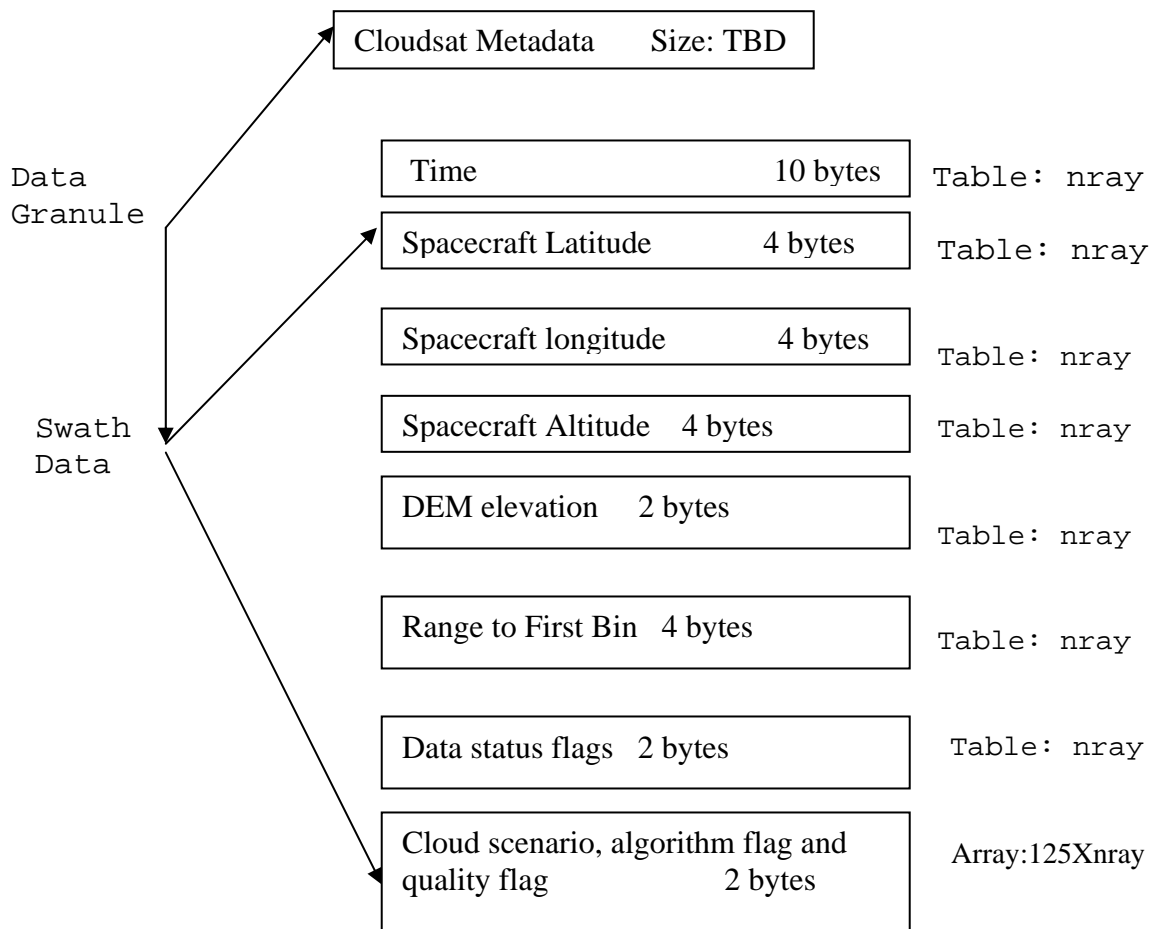


Figure 15. An example of cloud type classification with the CloudSat radar measurements. From top to bottom, panels are the CloudSat ground track plotted over a merged IR image between 60S and 60N collected around the time of the CloudSat overpass (a), cloud type classification results (b), cloud mask results (c), calibrated CPR radar reflectivity factor (d), and ECMWF temperature profiles under the CloudSat track (e). Note that occurrences of precipitation are indicated in (b) with lines below 0 km MSL.

5. Data Product Output Format

The format consists of metadata, which describes the data characteristics, and swath data, which includes cloud scenario at each range bin, as well as other information. The following schematic illustrates how cloud scenario data is formatted using HDF EOS. The variable *nray* is the number of radar blocks (frames, rays) in a granule. Each block is a 0.16 s average of radar data.

CloudSat Level 2 Cloud Scenario HDF-EOS Data Structure



5.1 Product Field Specifications

(Generated by AIMS on 24 July 2007)

Dimensions Used

nray (typical value: 36383) Number of CPR rays in one orbit.

nbin (typical value: 125) Number of vertical bins

(1) Seconds since the start of the granule.

Name in file: Profile_time **Range:** 0 to 6000
Source: 2B-GEOPROF 011 **Missing value:**
Field type (in file): REAL(4) **Missing value operator:**
Field type (in algorithm): REAL(4) **Factor:** 1
Dimensions: nray **Offset:** 0
Units: seconds **MB:** 0.139

Seconds since the start of the granule for each profile. The first profile is 0.

(2) UTC seconds since 00:00 Z of the first profile

Name in file: UTC_start **Range:** 0 to 86400
Source: 2B-GEOPROF 011 **Missing value:**
Field type (in file): REAL(4) **Missing value operator:**
Field type (in algorithm): REAL(4) **Factor:** 1
Dimensions: <scalar> **Offset:** 0
Units: seconds **MB:** 0

The UTC seconds since 00:00 Z of the first profile in the data file.

(3) TAI time for the first profile.

Name in file: TAI_start **Range:** 0 to 6e+008
Source: 2B-GEOPROF 011 **Missing value:**
Field type (in file): REAL(8) **Missing value operator:**
Field type (in algorithm): REAL(8) **Factor:** 1
Dimensions: <scalar> **Offset:** 0
Units: seconds **MB:** 0

The TAI timestamp for the first profile in the data file. TAI is International Atomic Time: seconds since 00:00:00 Jan 1 1993.

(4) Spacecraft Latitude

Name in file: Latitude **Range:** -90 to 90
Source: 2B-GEOPROF 011 **Missing value:**
Field type (in file): REAL(4) **Missing value operator:**
Field type (in algorithm): REAL(4) **Factor:** 1
Dimensions: nray **Offset:** 0
Units: degrees **MB:** 0.139

Spacecraft Geodetic Latitude.

(5) Spacecraft Longitude

Name in file: Longitude **Range:** -180 to 180
Source: 2B-GEOPROF 011 **Missing value:**
Field type (in file): REAL(4) **Missing value operator:**
Field type (in algorithm): REAL(4) **Factor:** 1
Dimensions: nray **Offset:** 0
Units: degrees **MB:** 0.139

Spacecraft geodetic longitude

(6) Height of range bin in Reflectivity/Cloud Mask above reference surface (~ mean sea level).

Name in file: Height **Range:** -5000 to 30000
Source: 2B-GEOPROF 011 **Missing value:** -9999
Field type (in file): INT(2) **Missing value operator:** ==
Field type (in algorithm): INT(2) **Factor:** 1
Dimensions: nbin,nray **Offset:** 0
Units: m **MB:** 8.674

Height of the radar range bins in meters above mean sea level.

(7) Range to the CPR boresight intercept with the geoid

Name in file: Range_to_intercept **Range:** 600 to 800

Source: 2B-GEOPROF 011 **Missing value:**
Field type (in file): REAL(4) **Missing value operator:**
Field type (in algorithm): REAL(4) **Factor:** 1
Dimensions: nray **Offset:** 0
Units: km **MB:** 0.139
 Range from the spacecraft to the CPR boresight intercept with the geoid.

(8) Digital Elevation Map

Name in file: DEM_elevation **Range:** -9999 to 8850
Source: 2B-GEOPROF 011 **Missing value:** 9999
Field type (in file): INT(2) **Missing value operator:** ==
Field type (in algorithm): INT(2) **Factor:** 1
Dimensions: nray **Offset:** 0
Units: meters **MB:** 0.069
 Elevation in meters above Mean Sea Level. A value of -9999 indicates ocean. A value of 9999 indicates an error in calculation of the elevation.

(9) CloudSat Bin size

Name in file: Vertical_binsize **Range:** to
Source: 2B-GEOPROF 011 **Missing value:** -9999
Field type (in file): REAL(4) **Missing value operator:** ==
Field type (in algorithm): REAL(4) **Factor:** 1
Dimensions: <scalar> **Offset:** 0
Units: m **MB:** 0
 effective vertical height of the radar range bin.

(10) Nominal satellite pitch angle offset from nadir

Name in file: Pitch_offset **Range:** -90 to 90
Source: 2B-GEOPROF 011 **Missing value:**
Field type (in file): REAL(4) **Missing value operator:**
Field type (in algorithm): REAL(4) **Factor:** 1
Dimensions: <scalar> **Offset:** 0
Units: degrees **MB:** 0
 The pitch angle offset from nadir during normal operations. Pitch up is positive (radar points along the flight track in the direction of motion), down is negative (radar points along the flight track opposite the direction of motion).

(11) Nominal satellite roll angle offset from nadir

Name in file: Roll_offset **Range:** -90 to 90
Source: 2B-GEOPROF 011 **Missing value:**
Field type (in file): REAL(4) **Missing value operator:**
Field type (in algorithm): REAL(4) **Factor:** 1
Dimensions: <scalar> **Offset:** 0
Units: degrees **MB:** 0
 The roll angle offset from nadir during normal operations. Positive roll results in the radar pointing to the right of the flight track. Negative roll to the left.

(12) Data Quality

Name in file: Data_quality **Range:** 0 to 127
Source: 2B-GEOPROF 011 **Missing value:**
Field type (in file): UINT(1) **Missing value operator:**
Field type (in algorithm): INT(2) **Factor:** 1
Dimensions: nray **Offset:** 0
Units: -- **MB:** 0.035
 Flags indicating data quality. If 0, then data is of good quality. Otherwise, treat as a bit field with 8 flags:

- 0: RayStatus_validity not normal.
- 1: GPS data not valid.
- 2: Temperatures not valid.
- 3: Radar telemetry data quality is not normal.
- 4: Peak power is not normal.
- 5: CPR calibration maneuver.
- 6: Missing frame.
- 7: Not used.

(13) Data status flags

Name in file: Data_status	Range: 0 to 127
Source: 2B-GEOPROF 011	Missing value:
Field type (in file): UINT(1)	Missing value operator:
Field type (in algorithm): UINT(1)	Factor: 1
Dimensions: nray	Offset: 0
Units: --	MB: 0.035

This is a bit field that contains data status flags:

- Bit 0: missing frame (0=false, 1=true)
- Bit 1: SOH missing (0=false, 1=true)
- Bit 2: GPS data valid (0=false, 1=true)
- Bit 3: 1 PPS lost (0=false, 1=true)
- Bit 4: Star tracker 1 (0=off, 1=on)
- Bit 5: Star tracker 2 (0=off, 1=on)
- Bit 6: Coast (0=false, 1=true)
- Bit 7: NISC (0=false, 1=true)

(14) CPR bus orientation (target ID)

Name in file: Data_targetID	Range: 0 to 81
Source: 2B-GEOPROF 011	Missing value:
Field type (in file): UINT(1)	Missing value operator:
Field type (in algorithm): INT(1)	Factor: 1
Dimensions: nray	Offset: 0
Units: --	MB: 0.035

The target id indicates the orientation of the spacecraft bus. For normal operations the target ID is 0. The complete ID table is listed below:

Control Frame 0

- 0: CPR to point in 300 seconds - Nominal science mode
- 1 - 15: Target ID for testing - not planned for operational use

Control Frame 0, CPR Calibration

- 16: CPR to point in 160 seconds
- 17: CPR 15° to the right
- 18: CPR 15° to the left
- 19: CPR 10° to the right -- default rotation
- 20: CPR 10° to the left -- default rotation
- 21: CPR 5° to the right
- 22: CPR 5° to the left
- 23 - 29: Target ID for testing - not planned for operational use

30 - 36: CPR rotation - not planned for operational use
37 - 39: Not planned for operational use

Control Frame 1, Four thruster closed-loop

40: Rotation into the OR orientation
41: Rotation into the x-track along the anti-ang momentum
42: Rotation into the x-track along ang momentum
43: Rotation into the orbit lower orientation
44: Rotation into alt. OR w/ CPR away from Sun
45 - 49: Not planned for operational use

Control Frame 2, One thruster open-loop

50: Rotation into the OR orientation
51: Rotation into the x-track along the anti-ang momentum
52: Rotation into the x-track along ang momentum
53: Rotation into the orbit lower orientation
54: Rotation into alt. OR w/ CPR away from Sun
55 - 59: Not planned for operational use

Control Frame 3, Two thruster open-loop

60: Rotation into the OR orientation
61: Rotation into the x-track along the anti-ang momentum
62: Rotation into the x-track along ang momentum
63: Rotation into the orbit lower orientation
64: Rotation into alt. OR w/ CPR away from Sun
65 - 69: Not planned for operational use

Control Frame 4, Four thruster open-loop

70: Rotation into the OR orientation
71: Rotation into the x-track along the anti-ang momentum
72: Rotation into the x-track along ang momentum
73: Rotation into the orbit lower orientation
74: Rotation into alt. OR w/ CPR away from Sun
75 - 80: Not planned for operational use

Control Frame 5

81: Body into the x-track along the anti-ang momentum
82 - 1023: Not planned for operational use

(15) Cloud scenario

Name in file: cloud_scenario	Range: 0 to 32767
Source: 2B-CLDCLASS 009	Missing value:
Field type (in file): INT(2)	Missing value operator:
Field type (in algorithm): INT(2)	Factor: 1
Dimensions: nbin,nray	Offset: 0
Units: none	MB: 8.674

Algorithm outputs (cloud type and different flags) are combined into a 16 bit cloud_scenario. See Table 5 for file specification for 16-Bit cloud scenario. The

precipitation flag indicates that the bin associated cloud layer has precipitation or not, and is not an indication for the bin.

Table 5. File Specification for 16-Bit cloud scenario

Bit Field	16 Bit Cloud Scenario File Specification	
	Description Key	Result
0	Cloud scenario flag	0 = not determined * 1 = determined
1-4	Cloud scenario	0000 = No cloud 0001 = cirrus 0010 = Altostratus 0011 = Altocumulus 0100 = St 0101 = Sc 0110 = Cumulus 0111 = Ns 1000 = Deep Convection
5-6	Land/sea flag	00 = no specific 01 = land 10 = sea 11 = snow (?)
7-8	Latitude flag	00 = tropical 01 = midlatitude 10 = polar
9-10	Algorithm flag	00 = radar only 01 = combined radar and MODIS
11-12	Quality flag	00 = not very confident 01 = confident
13-14	Precipitation flag	00 = no precipitation 01 = liquid precipitation 10 = solid precipitation 11 = possible drizzle
15	Spare	

* When cloud scenario is not determined, it may be caused by missing or bad critical inputs, such as radar reflectivity and temperature profiles. Data_status contains a flag for missing radar rays.

6. Operator Instructions

The Level 2 cloud scenario classification processing software will be integrated into CORE. It will be called using the standard CORE procedure for calling modules to operate on data files. The output will be in the form of an HDF-EOS structure in memory, which can be saved by CORE and passed on to other Level 2 processing.

This algorithm works at two different modes: radar only and combined radar and MODIS. If there are MODIS data and radar results indicate a single layer cloud system, algorithm selects the combined radar and MODIS mode, otherwise, algorithm uses radar only mode. But the combined radar and MODIS approach is still under development. The different modes are indicated in the outputs with algorithm flag.

For quality assessment purpose, statistics for cloud cover and height are generated. Average cloud covers within 300 CPR profiles are calculated for all clouds, high, middle (As and Ac), low (St, Sc and Cu) and thick (Ns and deep convective) clouds, respectively. The occurrence of multi-layer clouds can be seen from this statistics. The percentage of clouds masked by 2B-GEOPROF and analyzed in this algorithm is also given. It supposes to be 100%, and less than 100% means something wrong in the algorithm. The following is an example of output for cloud cover statistics form test data set 1.

```
***** Cloud Cover and Analysis Statistics *****
Index, Mean Lat, Mean Lon, Percentage of Cloud Mask Analyzed,
Cloud Cover:All, High, Mid, Low,and Thick Clouds
1 1.475 93.484 100.000 59.000 18.667 34.333 29.333 0.000
2 4.422 92.859 100.000 39.667 12.333 14.000 41.000 0.000
3 7.369 92.230 100.000 24.000 9.333 17.000 0.000 0.000
4 10.316 91.596 100.000 49.333 7.667 45.667 0.333 0.000
5 13.261 90.954 100.000 65.667 20.000 43.667 3.333 24.667
6 16.205 90.301 100.000 2.000 2.000 0.333 0.000 0.000
7 19.148 89.634 100.000 18.333 4.333 15.333 0.000 0.000
8 22.088 88.951 100.000 75.000 5.667 66.000 6.000 22.000
9 25.025 88.248 100.000 18.000 2.667 14.667 5.333 0.000
10 27.960 87.520 100.000 55.000 61.333 0.667 0.000 0.000
11 30.891 86.763 100.000 99.333 44.667 3.000 5.000 96.000
12 33.818 85.972 100.000 89.667 35.333 32.333 2.667 43.000
13 36.740 85.139 100.000 84.667 10.333 79.667 0.000 0.000
14 39.657 84.257 100.000 8.000 6.333 0.667 2.667 0.000
15 42.568 83.315 100.000 2.333 2.667 0.333 0.000 0.000
16 45.473 82.301 100.000 79.667 37.333 45.333 0.000 0.000
17 48.368 81.200 100.000 49.000 11.333 49.333 0.000 0.000
18 51.255 79.991 100.000 31.333 9.667 32.333 0.667 0.000
19 54.130 78.648 100.000 3.667 4.000 0.000 0.000 0.000
20 56.990 77.136 100.000 21.667 1.667 4.667 1.667 16.000
21 59.834 75.407 100.000 40.667 42.667 0.000 0.000 0.000
22 62.711 73.348 100.000 95.333 24.667 28.000 7.333 52.333
23 65.529 70.922 100.000 85.667 8.667 5.667 53.333 34.333
```

24	68.279	67.993	100.000	76.667	6.333	11.333	42.000	30.333
25	70.970	64.325	100.000	19.000	2.667	5.333	0.000	11.333
26	73.576	59.581	100.000	36.333	4.000	33.667	2.333	0.000
27	76.048	53.225	100.000	32.667	36.333	0.000	0.000	0.000
28	78.302	44.419	100.000	36.000	20.333	28.000	0.667	0.000

Cloud height statistics (mean, standard deviation, maximum, and minimum of cloud base and top heights) for different type clouds in different latitudes are also calculated. These results provide useful information when algorithm or input data have problems. For example, if results indicate that high clouds occur below 2 km above sea level, there is something wrong in the algorithm or input data. An example of output for test data set one is given below. Cloud types 1 to 8 represent high, As, Ac, St, Sc, Cu, Ns, and deep convective clouds, respectively.

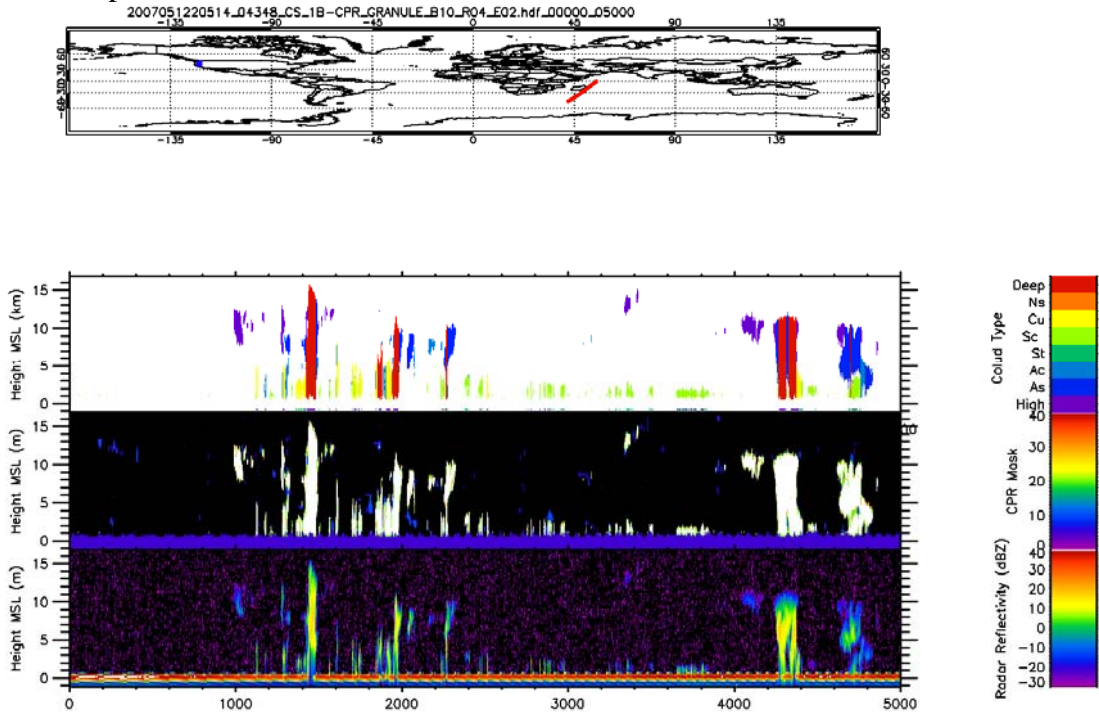
*****Cloud Height (base and top) Statistics for each type*****

Type	Mean	STD	Max	Min	
Whole Granule Average					
1	11.038	6.007	28.797	5.037	← Cloud base
1	12.381	5.560	28.917	5.157	← Cloud top
2	4.205	1.719	12.477	-0.003	
2	6.360	2.658	14.997	0.597	
3	3.353	1.467	9.597	-0.003	
3	4.305	1.634	10.437	0.597	
4	0.176	0.364	2.157	-0.003	
4	0.867	0.519	2.757	0.117	
5	0.370	0.450	3.597	-0.003	
5	1.531	0.711	5.637	0.117	
6	1.032	1.213	6.957	-0.003	
6	2.187	1.621	11.397	0.117	
7	0.418	0.835	3.357	-0.003	
7	4.429	2.105	13.077	1.557	
8	1.169	1.408	3.837	-0.003	
8	5.423	1.898	12.837	1.557	
Tropical Average ← -23.5 to 23.5					
1	13.059	5.730	28.797	5.037	
1	14.336	5.221	28.917	7.317	
2	4.887	1.829	9.837	0.717	
2	6.688	2.408	13.077	1.557	
3	3.786	1.949	9.597	-0.003	
3	5.390	2.171	10.437	2.757	
4	0.255	0.507	2.157	-0.003	
4	0.686	0.626	2.277	0.117	
5	0.507	0.539	2.637	-0.003	
5	1.467	0.813	4.917	0.117	
6	1.134	1.285	6.957	-0.003	
6	2.204	1.459	7.317	0.117	
7	0.420	0.737	3.357	-0.003	
7	4.325	1.394	9.477	1.557	
8	0.697	1.149	3.837	-0.003	
8	4.651	1.338	8.277	1.557	

	Subtropical Average				← -35 to -23.5 and 23.5 to 35
1	11.247	5.631	28.797	5.037	
1	12.561	5.283	28.917	5.397	
2	4.048	1.262	9.837	0.717	
2	5.275	1.549	13.317	2.037	
3	3.629	2.104	6.477	0.957	
3	4.133	2.168	6.837	1.077	
4	0.053	0.258	1.437	-0.003	
4	0.559	0.439	2.037	0.117	
5	0.849	0.571	3.597	-0.003	
5	1.701	0.501	3.957	0.357	
6	1.235	1.429	5.517	-0.003	
6	1.918	1.476	5.877	0.117	
7	0.250	0.625	3.357	-0.003	
7	3.710	1.704	9.477	1.557	
8	2.224	1.766	3.837	-0.003	
8	5.790	1.090	8.277	2.757	
	Midlatitude Average				← -55 to -35 and 35 to 55
1	11.213	6.676	28.797	5.037	
1	12.375	6.204	28.917	5.157	
2	4.218	1.245	12.477	1.437	
2	6.483	2.394	14.757	2.277	
3	3.338	0.737	5.277	0.237	
3	4.158	0.633	5.877	2.757	
4	0.077	0.274	1.437	-0.003	
4	0.782	0.428	2.037	0.117	
5	0.231	0.397	3.357	-0.003	
5	1.539	0.750	5.637	0.117	
6	0.824	1.124	6.477	-0.003	
6	2.011	1.548	7.557	0.117	
7	1.142	1.262	3.357	-0.003	
7	6.052	2.771	10.437	1.557	
8	1.651	1.359	3.837	-0.003	
8	5.462	1.660	10.677	1.797	
	High latitude Average				← -90 to -55 and 55 to 90
1	9.891	5.687	28.797	5.037	
1	11.356	5.260	28.917	5.157	
2	3.879	1.962	10.557	-0.003	
2	6.529	3.157	14.997	0.597	
3	2.877	1.193	5.037	0.237	
3	3.581	1.136	6.357	0.597	
4	0.216	0.282	2.157	-0.003	
4	1.161	0.329	2.757	0.357	
5	0.427	0.341	3.117	-0.003	
5	1.527	0.597	4.917	0.117	
6	0.999	1.093	5.517	-0.003	
6	2.374	1.814	11.397	0.117	
7	0.302	0.700	3.357	-0.003	
7	4.438	2.066	13.077	1.557	
8	0.808	1.227	3.837	-0.003	
8	5.710	2.310	12.837	1.797	

Another quick look for the performance of algorithm is to plot cloud type profile together with radar reflectivity and cloud mask profiles. An example of this plot is given in next

page. Horizontal and vertical distributions of cloud types can be easily examined from this kind of plot.



7. References

- Ackerman, S. A., K. I. Strabala, W. P. Menzel, R. A. Frey, C. C. Moeller, and L. E. Gumley, 1998: Discriminating clear sky from clouds with MODIS. *J. Geophys. Res.*, **32**,141-32,157.
- Bankert, R. L., 1994: Cloud classification of AVHRR imagery in maritime regions using a probabilistic neural network. *J. Appl. Meteor.*, **33**, 909-918.
- Chen, T., W. B. Rossow, and Y. Zhang, 2000: Cloud type radiative effects from the international satellite cloud climatology project. Proc. *11th Symposium on Global Change Studies*, Long Beach, California, American Meteorological Society, 86-89.
- Duchon, C. E., and M. S. O'Malley, 1999: Estimating cloud type from pyranometer observations. *J. Appl. Meteor.*, **38**, 132-141.
- Haynes, J. M., and G. L. Stephens, 2007: Tropical oceanic cloudiness and the incidence of precipitation: Early results from CloudSat. *Geophys. Res. Lett.*, **34**, L09811, doi:10.1029/2007GL029335.
- Hartmann, D. L., M. E. Ockert-bell, and M. L. Michelsen, 1992: The effect of cloud type on Earth's energy balance: global analysis. *J. Climate*, **5**, 1281-1304.
- Luo, G., P. A. Davis, L. L. Stowe, and E. P. McClain, 1995: A pixel-scale algorithm of cloud type, layer, and amount for AVHRR data. Part I: nighttime. *J. Atmos. Oceanic. Technol.*, **12**, 1013-1037.
- Moran, J. M., M. D. Morgan, and P. M. Pauley, 1997: *Meteorology: the Atmosphere and the Science of Weather*. Prentice-Hall, 530 pp.
- Parker, S. P., Editor in chief, 1988: *Meteorology Source Book*. McGraw-Hall, 304 pp.
- Penaloza, M. A., and R. M. Welch, 1996: Feature selection for classification of polar regions using a fuzzy expert system. *Remote Sens. Environ.*, **58**, 81-100.
- Rossow, W. B., and R. A. Schiffer, 1999: Advances in understanding clouds from ISCCP. *Bull. Amer. Meteor. Soc.*, **80**, 2261-2286.
- Matrosov, S. Y., T. Uttal, and D.A. Hazen, 2004: Evaluation of Radar Reflectivity-Based Estimates of Water Content in Stratiform Marine Clouds. *J. Appl. Meteor.*, **43**, 405-419.
- Tovinkere, V. R., and M. Penaloza, A. Logar, J. Lee, R. C. Weger, T. A. Berendes, and R. M. Welch, 1993: An intercomparison of artificial intelligence approaches for polar scene identification. *J. Geophys. Res.*, **98**, 5001-5016.
- Uddstrom, M. J., and W. R. Gray, 1996: Satellite cloud classification and rain-rate estimation using multispectral radiances and measures of spatial texture. *J. Appl. Meteor.*, **35**, 839-858.
- Wang J., and B. Geerts, 2003: Identifying drizzle within marine stratus with W-band radar reflectivity. *Atmos. Res.*, **69**, 1-27.
- Wang, Z. and K. Sassen, 2001: Cloud type and macrophysical property retrieval using multiple remote sensors. *J. Appl. Meteor.*, **40**, 1665-1682.
- Wang, Z. and K. Sassen, 2004: An improved cloud classification algorithm based on the SGP CART site observations. *The Fourteenth ARM Science Team Meeting*,

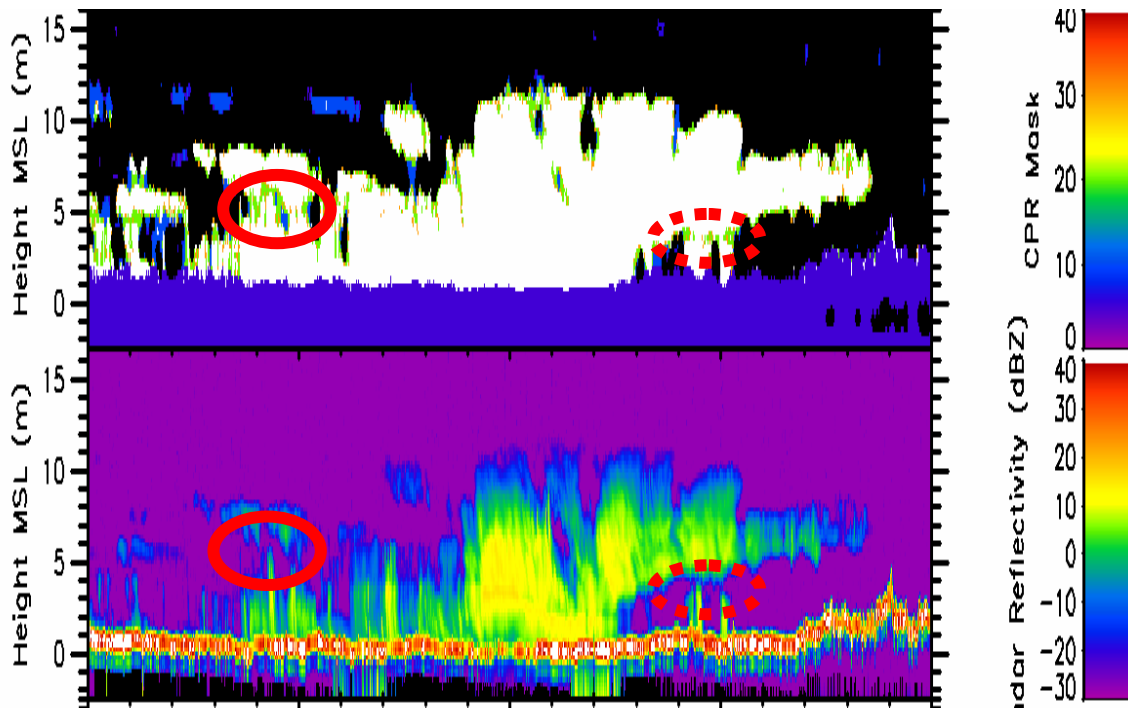
- March 22 to 26, 2004, Albuquerque, New Mexico,
<http://www.arm.gov/publications/proceedings.stm>.
- Welch, R. M., S. K. Sengupta, A. K. Goroch, P. Rabindra, N. Rangaraj, and M. S. Navar, 1992: Polar cloud and surface classification using AVHRR imagery: An intercomparison of methods. *J. Appl. Meteor.*, **31**, 405-420.
- Williams, C. R., W. L. Ecklund, and K. S. Gage, 1995: Classification of precipitating clouds in the tropics using 915-MHz wind profilers. *J. Atmos. Oceanic Technol.*, **12**, 996-1012.
- World Meteorological Organization, 1956: *International Cloud Atlas: abridged atlas*. WMO, Geneva [c1969].

8. Acronym List

Aqua	NASA's Earth Observing System PM Project
ARM	Atmospheric Radiation Measurement (ARM)
CIRA	Cooperative Institute for Research in the Atmosphere
CPR	Cloud Profiling Radar
CORE	CloudSat Operational and Research
EOS	Earth Observing System
HDF	Hierarchical Data Format
IFOV	Instantaneous field of view
IWC	Ice Water Content
LITE	Lidar In-space Technology Experiment
LWC	Liquid Water Content
MMCR	Millimeter- wave cloud radar
MODIS	Moderate Resolution Imaging Spectroradiometer
CALIPSO	Cloud-Aerosol Lidar and Infrared Pathfinder Satellite Observations
VTCW	Vehicle Time Code Word

9. Open Issues

- St and Sc are not well separated in this product. Reported St is low now. We are combining CloudSat Radar and CALIPSO lidar measurements to better understand the differences of St and Sc in terms of CloudSat radar signal globally in hoping to improve their separation with CloudSat only measurements. Thus it is better to combine St and Sc together for any boundary cloud study.
- High latitude cold near surface clouds might have slightly lower quality in general. One factor causing this is that CloudSat radar fails to provide the whole cloud structure due to small crystal size under cold and clean environment.
- There are few situations vertically connected layers (visually judged based on their horizontal structures) are regarded as one layer based on their vertical connection according to high confident cloud mask results, such as examples showed in the figure below (highlight with red circles). These situations either caused by weak precipitation from top layer or by cloud boundary stretch due to the long radar pulse or by cloud masking. We are able to separate simple cases, such as two well defined stratiform cloud layers connected by small portion of profiles. But there are still cases that we are unable to separate them correctly, which might result in wrong cloud type. However, these situations occurred at very low frequency, and you need to be aware of this if you look for a case study with CloudSat data.



10. Major changes since version 4.0

- 1) Precipitation identification is improved by selecting thresholds based on CloudSat measurements or detail analysis of ground-based observations.
- 2) To use bins recovered from surface cluster, cloud masks with values between 20 and 30 below the first cloud layer (identified with cloud mask ≥ 30) above surface are included in the analysis.
- 3) Cloud cluster analysis is improved to better group different cloud layer together.
- 4) Classification logic is adjusted based on CloudSat data over different regions and seasons.